FINITE ELEMENT AND POPULATION BALANCE MODELS FOR FOOD-FREEZING PROCESSES

by

MARK J. MILLER

B.S., Kansas State University, 2008

A THESIS

submitted in partial fulfillment of the requirements for the degree

MASTER OF SCIENCE

Department of Mechanical and Nuclear Engineering
College of Engineering

KANSAS STATE UNIVERSITY
Manhattan, Kansas

2010

Approved by:

Co-Major Professor
Dr. Jack Xin

Approved by:

Co-Major Professor
Dr. Z.J. Pei

Copyright

Abstract

Energy consumption due to dairy production constitutes 10% of all energy usage in the U.S. Food Industry. Improving energy efficiency in food refrigeration and freezing plays an important role in meeting the energy challenges of today. Freezing and hardening are important but energy-intensive steps in ice cream manufacturing. This thesis presents a series of models to address these issues. The first step taken to model energy consumption was to create a temperature-dependent ice cream material using empirical properties available in the literature. The homogeneous ice cream material is validated using finite element analysis (FEA) and previously published experimental findings. The validated model is then used to study the efficiency of various package configurations in the ice cream hardening process. The next step taken is to consider product quality by modeling the ice crystal size distribution (CSD) throughout the hardening process. This is achieved through the use of population balance equations (PBE). Crystal size and corresponding hardened ice cream coarseness can be predicted through the PBE model presented in this thesis. The crystallization results are validated through previous experimental study. After the hardening studies are presented, the topic of continuous freezing is discussed. The actual ice cream continuous freezing process is inherently complex, and therefore simplifying assumptions are utilized in this work. Simulation is achieved through combined computational fluid dynamics (CFD) and PBE modeling of a sucrose solution. By assuming constant fluid viscosity, a two-dimensional cross section is able to be employed by the model. The results from this thesis provide a practical advancement of previous ice cream simulations and lay the groundwork for future studies.

Table of Contents

List of Figures

List of Tables

Acknowledgements

I would like to thank my graduate committee: Profs. Jack Xin, Z.J. Pei, Karen Schmidt, and Sameer Madanshetty. I would also like to thank Will Cromer and Nick Rauth for the assistance they provided on this work. I am also grateful to ASME for the opportunity to present the work of Chapter 4 and portions of Chapter 3 at the 2010 Manufacturing Science and Engineering Conference (MSEC) in Erie, PA. Lastly I would like to thank my fellow graduate students who have enriched my education.

Chapter 1 - Introduction

1. Thesis Format

Following this introductory chapter, three technical chapters are presented. At the time of the thesis submission, Chapters 2 and 3 are in the process of being submitted to the International Journal of Refrigeration and Computational Materials Science, respectively. The fourth chapter was presented at the ASME 2010 Manufacturing Science and Engineering Conference (MSEC) in Erie, PA. The reference number for that paper is MSEC2010-34218. Also note that two other MSEC papers were presented on this work: MSEC2010-34103 and 34104. Appendix A provides complete references for each paper. The fifth chapter of this thesis summarizes conclusions and future research directions.

2. Thesis Overview

Ice cream manufacturing is comprised of several carefully-controlled steps. The following work addresses the freezing and hardening process steps through numerical simulation. The primary motivation for these analyses is to reduce energy consumption throughout the manufacturing process. Secondary goals include better fundamental understanding of the material science and improving quality control through ice crystal size prediction. To provide an adequate background and context for the present work, a literature review on ice cream manufacturing and related topics is presented in Section 3. Thesis goals are expanded in Section 4.

The second chapter develops a single phase, finite element model for energy analysis in the hardening process step. The model is validated using previously published experimental

results, and then specific energy saving approaches are presented and quantified. The third chapter advances the hardening model using the population balance (PB) method of Randolph and Larson (1988). This approach allows for greater microstructural representation. A multiphase material is used to predict the ice crystal size distribution (CSD) throughout the hardening process. The simulation is carried out using Fluent 6.3 (2006) for its heat transfer and PB capabilities. The material is assumed to be internally static in the blast freezer, and therefore flow calculations are not required.

The fourth chapter focuses on the continuous freezing process within a scraped surface heat exchanger (SSHE). The process is highly complex given the non-Newtonian, temperature-dependent viscosity of the ice cream mix. Chapter 4 takes a different approach to this step by using computational fluid dynamics (CFD) to model a sucrose solution instead of the ice cream mix. Flow characteristics are simulated using a constant sucrose solution viscosity. The ice CSD is predicted and compared with previous experimental and numerical work. Conclusions and future research are restated in the fifth chapter.

3. Literature Review

3.1. Ice Cream Manufacturing

3.1.1. Processing Stage 1

A typical ice cream mix is composed of 10% milk fat, 20% milk solids (including the 10% milk fat), 16% sweeteners, and 0.5% stabilizers and emulsifiers, with the remaining portion being water (Marshall et al., 2003). These ingredients will be combined and then blended, pasteurized, homogenized, and cooled (Fellows, 2000). Table 1.1 shows each of the

manufacturing steps with their associated process stages. The first process stage will result in a homogenous liquid mix which can then be converted to the partially frozen foam of many different flavors. To produce a high quality ice cream product, the homogenization process is important, as it breaks large fat globules into much smaller ones (from approximately 10 to 1 μm in diameter). This is achieved by forcing the globules through a series of small valves using pressures up to about 150 atm on the first stage and 35 atm on the second stage. This two-stage system reduces the propensity of fat globules to cluster. At the same time surface active components reorient and form a new membrane around the individual fat globules.

The cooled mix is then pumped into aging tanks. Several chemical reactions occur during aging that contribute to high-quality ice cream. First, the emulsifiers displace proteins and adsorb on the fat globule surfaces, forming a weaker membrane (Clarke, 2004). Second, the milk fat begins to crystallize. Most ice cream mixes require 2 to 6 hours to age properly.

3.1.2 Processing Stage 2

The second stage consists of flavoring and coloring, freezing, particulate addition, packaging, hardening, and storage. While the flavoring and coloring step provides the characteristic flavor and color to the ice cream mix, freezing is usually achieved by pumping 2 to 4°C mix into a scraped-surface heat exchanger (Marshall et al., 2003) to form the partially-frozen foam. In the freezer, the ice cream mix is vigorously agitated and cooled, and thin layers of ice form on the barrel wall. These crystals are removed by the dasher, and return to the mix along with air bubbles. The freezing process is maintained at a relatively high rate, because this supports the greatest amount of nucleation (Goff, 2009). Agitation also causes the fat globules to partially coalesce, and that in turn allows them to capture the air bubbles within the fat crystal

networks. Together these components create the colloidal foam of ice cream. A useful review of ice cream structure formation and stabilization is available from Goff (2002). Processing time for continuous freezers is typically on the order of 30 seconds and during this time about 50% of water in the mix is frozen.

Ice cream exits the freezer at -5 to -6°C with 20 to 60% fat destabilization (Marshall et al., 2003). Particulates such as nuts or fruits are sometimes added after the processing step, but all ice cream will be quickly packaged and will undergo the hardening process. Hardening is usually performed in a tunnel with airflow at -30 to -45°C. The final product emerges between about -15 and -20°C (Schmidt, 2004).

3.2. Energy Usage

Nearly six billion liters of ice cream and related frozen desserts were produced in the United States in 2006. Total sales for the year were close to $23 billion (IDFA, 2009). Energy consumption by the U.S. dairy industry was 121 Trillion Btu (35B kW·h). This is equivalent to 11 months of electricity consumption for the state of Kansas in 2006 (EIA, 2006). This usage constitutes 10.2% of all energy consumed by the U.S. food industry (EIA, 2006). Consequently, manufacturers are becoming increasingly interested in strategies to reduce energy needs (Higgins, 2009).

Ice cream manufacturing requires several meticulous steps. These have been discussed in the preceding section and are detailed at length by Marshall et al. (2003), as well as Schmidt (2004) and Clarke (2004). Freezing, hardening, and storage make up the most significant energy usage (Greener, 2010), and all three involve refrigeration. Ice cream studies have been predominantly experimental with focus on the freezing process (Adapa et al., 2000; Flores and

Goff, 1999; Russell et al., 1999; Donhowe et al., 1991; Bolliger et al., 2000). Specific ice cream energy studies are quite limited. One of the few ice cream energy efficiency studies available in the literature is an experimental study by Smith et al. (1985). That work considered the effect of sweeteners and gums on the electrical energy requirements of the freezing process. Energy simulations are also few in number. One example is the continuous freezer heat transfer model of Bongers (2006).

Although hardening is actually the most energy intensive step, consuming roughly 45% of the total energy in ice cream manufacturing (Greener, 2010), little has been published on energy consumption during the process. Air temperatures in the hardening room may be lower than -35°C, yet it can take hours for the ice cream to reach the required temperature of -18°C (Marshall et al., 2003). Tracey and McCown (1934) experimentally studied the effects of forced convection and packaging. De Cindio et al. (1985) investigated the ice cream hardening using a 2D transient finite element analysis. Rauth et al. (2010) used a three-dimensional FEA model to replicate the experimental hardening results of Tracey and McCown (1934). Cromer et al. (2010) studied energy efficiency in the hardening process by varying package configurations. Temperature fluctuations of the subsequent process, storage, were modeled by Zuritz and Singh (1985).

3.3. Crystallization

The main difficulty in modeling ice cream is its complex microstructure. In order for meaningful conclusions on energy efficiency to be drawn, product quality (texture) must be considered. This means that the microstructure must be accounted for in some regard. While each individual step is required to achieve an acceptable mouthfeel (texture), the freezing and

hardening processes have the greatest impact on the ice cream microstructure. Crystals form and grow in order to alleviate undercooling during these refrigeration steps (Fennema et al., 1973; Sutton and Bracey, 1996). Substantial research has been conducted in this field, but much uncertainty remains due to the inherent complexity of the crystallization kinetics (Cook and Hartel, 2010). Most ice crystallization studies have focused on experimental investigation, rather than computational modeling.

Experimental ice cream research includes an extensive study by Russell et al. (1999) to determine the most dominant crystallization mechanisms within an SSHE. They also briefly considered the conventional hardening process. Adapa et al. (2000) reviewed the influence of fat content and fat replacers on the viscoelastic properties of ice cream. Crilly et al. (2008), as well as Regand and Goff (2005), studied the effects of ice structuring proteins (ISPs). Recrystallization has been discussed by Donhowe and Hartel (1996), and ice recrystallization inhibition was studied by Aleong et al. (2008). Other innovations include the low temperature extrusion (LTE) process detailed by Wildmoser et al. (2004). Their work showed that the twin screw extrusion system (TS-LTE) resulted in significant quality improvements over the conventional SSHE / hardening combination. As reviewed by Zheng and Sun (2006), ultrasound vibrations have been used to break up ice crystals during food freezing processes, including ice cream.

In contrast to the quickly developing experimental research, ice cream freezing and hardening simulations are fewer in number. Aldazabal et al. (2006) performed a hardening simulation in which sugar diffusion and ice crystal microstructure were modeled. Ben-Yoseph and Hartel (1998) simulated recrystallization during ice cream storage. A popular approach for simulating particulate processes is through the use of the population balance equations (PBE)

presented by Hulburt and Katz (1964) and refined for continuous crystallization by Randolph and Larson (1988). Examples of PBE simulations include those of Hey and MacFarlane (1998); Shirai et al. (1986). Some researchers have combined PBE with computational fluid dynamics (CFD) to model dynamic crystallization processes. Woo et al. (2006) modeled antisolvent crystallization in an agitated semibatch vessel using combined CFD-PBE. Similarly, Lian et al. (2006) simulated the crystallization of a sucrose solution within an SSHE using this method. PBE have also been applied to lactose crystallization by Griffiths et al. (1982); Shi et al. (1990). *Engineering Aspects of Milk and Dairy Products* provides a wealth of information on dairy crystallization topics (dos Reis Coimbra and Teixeira, 2010).

4. Summary of Thesis Goals

The primary goal of this work is to advance current energy and material simulations of ice cream manufacturing. To achieve this aim, the following intermediate goals have been developed.

1. Create a robust and accurate single phase ice cream material for FEA and CFD simulations.
2. Validate the single phase ice cream material with experimental results.
3. Utilize the validated hardening model to quantify process efficiency and to develop energy saving strategies.
4. Advance the single phase material to include multiphase ice CSD prediction in the hardening process.
5. Also use the multiphase approach to study the continuous freezing process.

References for Chapter 1

Adapa S, Schmidt KA, Jeon IJ, Herald TJ, Flores RA. 2000. Mechanisms of ice crystallization and recrystallization in ice cream: a review. Food Rev Int 16:259–71.

Aldazabal J, Martin-Meizoso A, Martinez-Esnaola JM, Farr R. 2006. Deterministic model for ice cream solidification. Comp Mat Sci 38:9-21.

Aleong JM, Frochot S, Goff HD. 2008. Ice recrystallization inhibition in ice cream by propylene glycol monostearate. J Food Sci 73:463–8.

Ben-Yoseph E, Hartel RW. 1998. Computer simulation of ice recrystallization in ice cream during storage. J Food Eng 38:309-29.

Bolliger S, Kornbrust B, Goff HD, Tharp BW, Windhab EJ. 2000. Influence of emulsifiers on ice cream produced by conventional freezing and low-temperature extrusion processing. Int Dairy J 10:497–504.

Bongers PMM. 2006. A Heat Exchanger Model of a Scraped Surface Heat Exchanger for Ice Cream. 16th European Symp Comp Aided Proc Eng and 9th Int Symp Proc Sys Eng. Ed. Marquardt W, Pantelides C. Published by Elsevier BV.

Cindio DB, Iorio G, Romano V. 1985. Thermal analysis of the freezing of ice cream brickettes by the Finite Element Method. J Food Sci 50:1463–6.

Clarke C. 2004. The Science of Ice Cream. Cambridge, UK: Royal Society of Chemistry.

Cook KLK, Hartel RW. 2010. Mechanisms of Ice Crystallization in Ice Cream Production. Compr Rev Food Sci Food Safety 9:213-22.

Crilly JF, Russell AB, Cox AR, Cebula DJ. 2008. Designing Multiscale Structures for Desired Properties of Ice Cream. Ind Eng Chem Res 47:6362-7.

Cromer WC, Miller MJ, Xin XJ, Pei ZJ, Schmidt KA. Effects of Container Geometry on Energy Consumption During Hardening in Ice Cream Manufacturing. Proc MSEC 2010, Ed. ASME, Erie, Pennsylvania, USA, 2010 Oct 12-15th.

Donhowe DP, Hartel RW, Bradley RL Jr. 1991. Determination of ice crystal size distributions in frozen desserts. J Dairy Sci 74:3334-44.

Donhowe DP, Hartel RW. 1996. Recrystallisation of ice cream during controlled accelerated storage. Int Dairy J 6:1191-208.

Energy Information Administration [Internet]. 2006 Energy consumption by manufacturers – data tables [Accessed 2009 Oct 1]. Available from:

http://www.eia.doe.gov/emeu/mecs/contents.html.

Fellows PJ. 2000. Food Processing Technology Principles and Practices. 2nd ed. New York: CRC Press.

Fennema OR, Powrie WD, Marth EH. 1973. Low-temperature Preservation of Foods and Living Matter. New York: Marcel Dekker.

Flores AA, Goff HD. 1999. Ice crystal size distributions in dynamically frozen model solutions and ice cream as affected by stabilizers. J Dairy Sci 82:1399-407.

Fluent Inc. 2006. Fluent 6.3. Lebannon, NH.

Goff HD. 2002. Formation and Stabilisation of Structure in Ice-Cream and Related Products. Curr Opinion Colloid Interface Sci 7:432-7.

Goff HD. 2009. [http://www.foodsci.uoguelph.ca/dairyedu] Accessed on 1/15/2010.

Greener RC. 2010. Rapid hardening systems [Accessed 2009 Dec 1]. Available form: http://www.freestech.com/img/Hardening%20And%20Storage%20Lecture2009.ppt

Griffiths RC, Paramo G, Merson RL. Preliminary Investigation of Lactose Crystallization Using the Population Balance Technique. AIChE Symposium Series 218:118-128.

Hey JM, MacFarlane DR. 1998. Crystallization of Ice in Aqueous Solutions of Glycerol and Dimethyl Sulfoxide 2: Ice Crystal Growth Kinetics. Cryobiology 37:119-30.

Higgins KT. 2009. Get smart about energy usage. Food Eng Magazine. 2009. Available from: http://www.foodengineeringmag.com.

Hulburt HM, Katz S. 1964. Some Problems in Particle Technology - a Statistical Mechanical Formulation. Chem Eng Sci 19:555-74.

IDFA. Dairy Facts. 2009 ed. International Dairy Foods Association. Washington DC.

Marshall RT, Goff HD, Hartel RW. 2003. Ice Cream. 6th ed. New York: Kluwer Academic/Plenum Publishers.

Randolph AD, Larson MA. 1988. Theory of Particulate Processes. 2nd ed. New York: Academic Press.

Rauth NL, Miller MJ, Xin XJ, Pei ZJ, Schmidt KA. Effects of Air Flow, Draw Temperature and Boundary Conditions on Hardening in Ice Cream Manufacturing. Proc MSEC 2010, Ed. ASME, Erie, Pennsylvania, USA, 2010 Oct 12-15th.

Regand A, Goff HD. 2005. Freezing and Ice Recrystallization Properties of Sucrose Solutions Containing Ice Structuring Proteins from Cold-Acclimated Winter Wheat Grass Extract. J Food Sci 70:E552-6.

Reis Coimbra DJS, Teixeira JA. 2010. Engineering Aspects of Milk and Dairy Products. Boca Raton, FL: CRC Press Taylor and Francis Group, LLC.

Russell AB, Cheney PE, Wantling SD. 1999. Influence of freezing conditions on ice crystallization in ice cream. J Food Eng 39:179–91.

Schmidt KA. 2004. Dairy: Ice Cream. In: Smith JS, Hui YH, editors. Food Processing Principles and Applications.1st ed. Iowa: Blackwell Publishing.

Shi Y, Liang B, Hartel RW. Crystallization Kinetics of Alpha-Lactose Monohydrate in a Continuous Cooling Crystallizer. J Food Sci 55:817-20.

Shirai Y, Sakai K, Nakanishi K, Matsuno R. 1986. Analysis of Ice Crystallization in Continuous Crystallizers Based on a Particle Size-dependent Growth Rate Model. Chem Eng Sci 41:2241-6.

Smith DE, Bakshi AS, Gay SA. 1985. Changes in Electrical Energy Requirements to Operate and Ice Cream Freezer as a Function of Sweeteners and Gums. J Dairy Sci 68:1349-51.

Sutton R, Bracey J. 1996. The blast factor. Dairy Industries Int 61:31-33.

Tracey PH, McCown CY. 1934. A study of factors related to the hardening of ice cream. J Dairy Sci 17:47-60.

Wildmoser H, Scheiwiller J, Windhab EJ. 2004. Impact of Disperse Microstructure on Rheology and Quality Aspects of Ice Cream. Lebensm-Wiss Technol 37:881-91.

Woo XY, Tan RBH, Chow PS, Braatz RD. 2006. Simulation of Mixing Effects in Antisolvent Crystallization Using a Coupled CFD-PDF-PBE Approach. Cryst Growth Des 6:1291-303.

Zheng L, Sun DW. 2006. Innovative Applications of Power Ultrasound During Food Freezing Processes - a Review. Trends Food Sci Tech 17:16-23.

Zuritz CA, Singh RP. 1985. Modelling temperature fluctuations in stored frozen food. Int J Refrig 8:289-93.

Table 1.1 Ice Cream Manufacturing

Processing Stage	Manufacturing Step
Stage 1	Blending Pasteurization Homogenization Cooling and Aging
Stage 2	Flavoring and Coloring Freezing Particulate Addition Packaging Hardening Storage

Chapter 2 - Finite Element Analysis of Ice Cream Hardening

Abstract

Energy consumption by the dairy industry in the United States constitutes 10% of all energy consumed by the U.S. food industry. Reducing energy consumption in cooling and refrigeration of foods plays an important role in meeting the energy challenges of today. Hardening is an important but energy-intensive step in ice cream manufacturing. This paper presents a finite element analysis (FEA) investigation of the ice cream hardening process. Temperature dependent ice cream properties were retrieved from published data, and FEA results were compared with previously published experimental results. The simulation shows how the most energy efficient processing variables can be determined. The effects of package configuration, heat transfer coefficient, and draw temperature on hardening time and energy efficiency were investigated.

1. Introduction

In the United States, close to six billion liters of ice cream and related frozen desserts were produced in 2006. The year saw total sales of nearly $23 billion (IDFA, 2009). In the same year, energy consumption by the dairy industry in the U.S. was 121 Trillion Btu, constituting 10.2% of all energy consumed by the U.S. food industry (EIA, 2006). Manufacturers are becoming more interested in ways to reduce energy consumption in their facilities (Higgins, 2009). The goal of this paper is to generate fundamental knowledge of ice cream hardening and

provide insight for energy savings in ice cream manufacturing, as well as other food freezing and storage processes.

Ice cream manufacturing involves numerous carefully controlled steps which have been thoroughly detailed by Marshall et al. (2003), as well as Schmidt (2004) and Clarke (2004). Freezing, hardening, and storage comprise the greatest energy usage (Greener, 2010), and all three process steps share the need for refrigeration. Studies on ice cream manufacturing have been predominantly experimental with focus on the freezing process (Adapa et al., 2000; Flores and Goff, 1999; Russell et al., 1999; Donhowe et al., 1991; Bolliger et al., 2000). Only limited computational models have been presented for any of these steps in the literature. Most studies on freezing have focused on the mechanisms of crystallization through experimentation as reviewed by Adapa et al. (2000), and demonstrated by Flores and Goff (1999); Russell et al. (1999).

Hardening is important to achieve an acceptable mouthfeel (texture). Very few crystals are formed during hardening since undercooling is mainly relieved by the growth of existing ice crystals (Fennema et al., 1973; Sutton and Bracey, 1996). Although the air temperature in the hardening room may be lower than -35°C, it can take hours for the ice cream to reach -18°C (Marshall et al., 2003). Tracey and McCown (1934) experimentally studied the effects of forced convection and packaging. De Cindio et al. (1985) investigated the hardening of ice cream using a 2D transient finite element analysis. Aldazabal et al. (2006) simulated the crystallization of an unaerated (no air incorporation) ice cream mix. Temperature fluctuations of the subsequent process, storage, were modeled by Zuritz and Singh (1985), and recrystallization was modeled by Donhowe and Hartel (1996); Ben-Yoseph and Hartel (1998). Ice recrystallization inhibition was studied by Aleong et al. (2008). Although hardening is actually the most energy intensive

step, consuming roughly 45% of the total energy in ice cream manufacturing (Greener, 2010), little has been published on energy consumption during the process.

The current work aims to achieve a better understanding of ice cream hardening using finite element analysis (FEA) and theoretical study, which can eventually be used to develop strategies for more efficient energy usage in a manufacturing site. The work addresses the following questions on ice cream hardening:

(a) How well can the process be modeled assuming ice cream as a homogeneous, solid material?

(b) How do the heat transfer boundary conditions affect the time required for hardening (residence time) and corresponding energy usage?

(c) How do the size and shape of the ice cream affect its residence time?

(d) Does an optimal hardening condition exist, and if so, how is it determined?

A series of FEA models were used to answer these questions. A rectangular model was studied to compare with a previously published simulation (de Cindio et al., 1985), and a cylindrical model was utilized to compare with previously published experimental data (Tracy and McCown, 1934). These comparisons helped establish the accuracy of the simulations. Further studies were then carried out to investigate the effects of boundary condition, container layer, ice cream package configuration, heat transfer coefficient, and draw temperature. The draw temperature is defined as the temperature of the ice cream product when exiting the freezer and before going into the hardening chamber. These models are described in Section 2, and the simulation results are discussed in Section 3. An optimal hardening condition was explored, and energy consumption was also considered. Conclusions are stated in Section 4.

2. Materials and Methods

2.1 Governing Equations

A number of assumptions were made in this study, including the following:

(1) The ice cream is a homogeneous, isotropic material.

(2) Phase changes in the ice cream are captured implicitly through temperature dependent material properties including heat conductivity and specific heat capacity.

(3) The convective heat transfer coefficient and the mass density remain constant during hardening.

For ice cream with 15% cane sugar, about 35% of the water was frozen at -3.9°C (25°F), and 82% was frozen at -17.8°C (0°F) (Tracy and McCown, 1934). Therefore, strictly speaking, the ice cream is not a solid, and localized heat convection may occur during the hardening process. However, without shearing and other mechanical agitation, the ice cream behaves much like a solid. Assumption (1) is therefore reasonable. With assumption (2), temperature dependent material properties represent the "smeared out" ice cream properties. While assumptions (1) to (3) are approximations of the real manufacturing conditions, they capture the essence of the heat transfer phenomenon in hardening, while simplifying the model.

The classical heat transfer equation for the problem is

$$k(T)\left[\frac{\partial^2 T}{\partial x^2}+\frac{\partial^2 T}{\partial y^2}+\frac{\partial^2 T}{\partial z^2}\right]-\rho C_p(T)\frac{\partial T}{\partial t}=0 \qquad (2.1)$$

where x, y and z are the Cartesian coordinates, t is time, T is the temperature which changes with position and time, i.e., $T=T(x,y,z;t)$, $k(T)$ is the temperature dependent thermal

conductivity, ρ is the mass density, and $C_p(T)$ is the temperature dependent specific heat capacity. In this work, a commercial Finite Element solver, SolidWorks Simulation (SolidWorks, 2010), was used to simulate the heat transfer process. The model development is as follows: (1) 2D rectangle; (2) 3D cylinder; (3) 3D sqround. Sqround, also squround, is an industry term that describes the hybrid square/round ice cream carton that eliminates sharp corners and provides easier scooping.

2.2 FEA Models

Density of the material was assumed constant at 500 kg/m^3. This is based on the work of de Cindio et al. (1985). The temperature dependent thermal conductivity was retrieved from the experimental data presented by Cogne et al. (2003), and specific heat capacity was from Cordell and Webb (1972). Thermal conductivity ranged from 0.48 W/(m·K) at -25^{o}C to 0.2 W/(m·K) at 0^{o}C. The heat capacity had the following characteristics: at -30^{o}C or lower it had a value of about 2 kJ/(kg·K), which is also the heat capacity for ice. Above -30^{o}C it rose rapidly, and spiked during the phase change; reaching a maximum of approximately 84 kJ/(kg·K) at 0^{o}C. It then abruptly transitioned to about 4 kJ/(kg·K) for temperatures above 0^{o}C. Table 2.1 shows the temperature dependent ice cream properties.

2.2.1 Model 2.1: Two-Dimensional, Quarter-Rectangle without Container

Model 2.1 was used to compare with the numerical results of de Cindio et al. (1985). This model represents a rectangular ice cream section. The dimensions for the ice cream geometry were 166 mm by 84 mm. Two planes of symmetry permitted the use of a one-quarter model of size 83 mm by 42 mm. The container was excluded; thus Model 2.1 represented the ice cream only. A shell mesh with an element size of 3.80 mm was used. This resulted in 484 elements.

Convection was applied to the two outer edges, while the symmetric (interior) edges were adiabatic. The initial temperature of the ice cream was uniformly -6°C, and the air temperature was -34°C. Three values of the convective coefficient, 63, 210, and 630 W/(m^2·K), were used for comparison with the results of de Cindio et al. (1985).

2.2.2 Model 2.2: Three-Dimensional, Eighth-Cylinder with Container

Model 2.2 was created to compare with the experiments of Tracy & McCown (1934). Their contributions included numerous configurations of 19 L (5 gal) ice cream volumes with forced and free convective conditions. They obtained measurements using copper-constantan thermocouples accurate within 0.1°F (Tracy and McCown, 1934). The models in this study were validated using their results. The height of the cylindrical model was 508 mm, and the diameter was 217.8 mm. A one-eighth model was employed to utilize symmetry. Figure 2.1 shows the geometry and mesh of the ice cream and container. The ice cream was modeled using second order solid elements, while the container was modeled as a 1 mm thick surface using second order shell elements. Both the solid and shell meshes had an average element size of 12.7 mm; resulting in a total of 16688 elements.

The container material was an alloy steel (Tracy and McCown, 1934) with a thermal conductivity of 45.3 W/(m·K). A specific heat of Cp = 460 J/(kg·K) was used. The ice cream thermal properties themselves were not studied by Tracy and McCown (1934). This led to the use of the properties listed in Table 2.1. While the mixture compositions were slightly different, the overall material behavior was very similar. A convective boundary condition was applied to all outer surfaces of the ice cream container, while adiabatic boundary conditions were applied to the symmetric planes of the one-eighth model. The bulk ambient temperature was -30°C (-22°F). Convective coefficients of 30, 40, and 63 W/(m^2·K) were used.

2.2.3 Model 2.3: Three-Dimensional, Quarter-Sqround with Container

Model 2.3 was motivated by the increased popularity of the sqround shape. Here a 1.66 L sqround with container was modeled. The solid model was created by scanning the top surface of an actual sqround and extruding it to a depth of 98 mm. The model was then drafted inward about the top edge at an angle of 5.46°. Figure 2.2 illustrates the sqround geometry, and Table 2.3 provides details about the geometric parameters of the sqround. Two planes of symmetry allowed for the use of a one-quarter model. Second order solid elements were used for the ice cream, and second order shell elements for the container. The average size of the solid and shell elements was 6.59 mm, which resulted in 16199 total elements for the quarter-model. Material properties are listed in Tables 2.1 and 2.2. Boundary conditions were similar to Model 2.1.

2.2.4 Models 2.4 and 2.5: Sqrounds with Holes

Since ice cream is a poor heat conductor, having a central hole in the sqround may help cool the ice cream more quickly. This was tested with Models 2.4 and 2.5. Model 2.4 was created by placing a 30 mm diameter hole (Hole 1) in the center of Model 2.3. To make up for the volume lost due to the hole, a scaling factor was used to maintain the volume of the original. Two symmetric planes permitted the use of a quarter model. Second order solid elements with an average size of 7 mm resulted in a total of 8188 elements. Conditions were similar to Model 2.3. Model 2.5 increased the hole of Model 2.4 to a 50 mm diameter.

2.2.5 Models 2.6 and 2.7: Reduced Heights

These models were used to investigate how much time and energy could be saved if an individual sqround was hardened in subcomponents. Portions of two halves and four quarters were considered. Model 2.6 was created by reducing the original Model 2.3 to half its height and

maintaining all of its conditions. The container was omitted. A smaller element size of 5.75 mm resulted in a total of 8648 elements. The quarter height Model 2.7 was created by cutting the original Model 2.3 into one quarter of its height and maintaining all of its conditions. Again, the container was omitted. A smaller element size of 4.55 mm resulted in a total of 8624 elements.

2.3. Mesh Refinement, Convective Coefficient, and Time Step

For all models, the element size was progressively refined and the model was re-analyzed to ensure numerical accuracy. A model was regarded as converged when temperature changes caused by mesh refinement were below 0.5%. The element sizes reported for all models were for converged meshes.

Convective coefficients of 63, 210, and 630 W/(m^2·K) were used in the work of de Cindio et al. (1985). However, the value was estimated to be about 23 W/(m^2·K) using parameters typical of an actual hardening process. This is detailed in Appendix B. This value agrees well with the range of 25 to 30 W/(m^2·K) presented by Fellows (2000). For parametric study, however, convective coefficients from 0.1 to 1000 W/(m^2·K) were used to investigate a wider range.

Time discretization scheme was based on the Fourier Number. Details of this dimensionless parameter can be found elsewhere (Incropera et al., 2007). Critical time steps in this study ranged from 50 to 300 sec.

3. Results and Discussion

3.1 Model Results

For conciseness, the dimensionless temperature θ is defined as:

$$\theta = \frac{T_t - T_\infty}{T_i - T_\infty} \tag{2.2}$$

where T_t is the ice cream temperature at a given time, T_∞ is the bulk ambient temperature, and T_i is the initial ice cream temperature.

3.1.1 Model 2.1 Results

The 2D results agreed well with those of de Cindio et al. (1985). Figure 2.3 shows the temperature evolution of the ice cream center. A total of 6000 sec (1.67 hr) was simulated for the shell mesh. Results from de Cindio et al. (1985) are shown as data markers for comparison. The discrepancy with the results of de Cindio et al. (1985) was less than 5%. A significant temperature change occurs within an hour of residence time. For a convective coefficient of 63 W/(m^2·K), the center dimensionless temperature θ reaches 0.5 (-20°C) in about 5220 sec (1.45 hr).

3.1.2 Model 2.2 Results

Three locations within Model 2.2 were selected for temperature monitoring. They were the radial center, midpoint, and outside of the mid-plane between the top and bottom of the container. These were designated as the center, middle circumference, and outer circumference. Figure 2.4 shows the evolution of these temperatures with time for a convective coefficient of 30 W/(m^2·K). The center temperature remained unchanged for about 15000 sec (4 hr 10 min) before decreasing to -17.8°C (0°F) at 24000 sec (6 hr 40 min). Note that lengthy hardening time resulted from the large volume of the cylinders 19 L (5 gal). The actual experimental values were 14400 sec (4 hr) for the center to begin changing and 22320 sec (6 hr 12 min) to reach -17.8°C (0°F) (Tracy and McCown, 1934). This shows that there was less than roughly 8% discrepancy

between the studies. The temperature at the outer circumference cooled rapidly almost from the start, while the middle circumference temperature behaved somewhere in between. Figure 2.5 shows the temperature contours in the FEA model after 3900 sec (1 hr 5 min). The center temperature remained at -4.78°C (23.4°F) at 3900 sec, while the edge temperature had reached approximately -24.4°C (-12°F). The simulation was repeated with convective coefficients of 40 and 63 W/(m^2·K). Figure 2.6 shows a comparison of the simulated center temperature with the experimental results (Tracy and McCown, 1934). Overall, 40 W/(m^2·K) curve fits the experimental data most closely.

3.1.3 Model 2.3 Results

Once the FEA models were validated, Model 2.3 was created to investigate the effects of geometry, convective coefficient, boundary conditions, and draw temperature. Convection was applied to all surfaces except for the bottom (which was adiabatic). Three convective coefficients were used: 30, 210, and 630 W/(m^2·K). 30 W/(m^2·K) was considered more representative of the realistic hardening conditions than 63 W/(m^2·K); a representative convective coefficient calculation can be found in Appendix B. The temperature variation of the mid-center of the sqround is shown in Figure 2.7. At 6000 sec (1.67 hr), the mid-center reached a temperature of θ = 0.418 (-22.3°C) and θ = 0.357 (-24.0°C) for 210 and 630 W/(m^2·K) respectively.

For a convective coefficient of 30 W/(m^2·K), the mid-center reached a dimensionless temperature of θ = 0.84 (-10.3°C) in about 6000 sec (1.67 hr). This indicates that the necessary residence time is probably closer to 2 hr. This corresponds well to field-observed dwell times of 1 to 2 hrs reported by Clarke (2004).

These results have other implications such as the likelihood of recrystallization to occur in areas which remain warmer for longer periods of time. Figure 2.2 shows temperature contours

of the center section of the sqround at 5400 sec (1.5 hrs). Note how the upper edge of the volume is clearly approaching the ambient temperature more quickly than the other regions. This aligns well with physical intuition about temperature changes in the product. Figure 2.8 shows the progression of the horizontal temperature distributions for a convective coefficient of 30 W/(m^2·K). The temperatures are taken along the major horizontal axis from the mid-center to the outer surface center at three selected time steps: 1800, 3600, and 5400 sec (0.5, 1, and 1.5 hrs). The figure reveals that at the first selected time step, 1800 sec, the surface temperature had already dropped to about -20^{o}C, while even after 5400 sec the mid-center temperature was still around -8^{o}C. For a convective coefficient of 210 W/(m^2·K), the mid-center temperature was θ = 0.58 (-17.8^{o}C) at 5400 sec. For 630 W/(m^2·K), the mid-center temperature reached θ = 0.52 (-19.4^{o}C) at 5400 sec.

The temperature decay results for the two larger coefficients are similar. Although there is a 3-fold increase in the convective coefficient, the mid-center temperature decreases by only 8.6% more for the largest coefficient. The low thermal conductivity of the ice cream dominates the hardening process. Newton's Law of Cooling dictates that heat transfer between an object and its environment is proportional to their temperature difference. The initial transfer rates are high, especially for larger convective coefficients, but drop rapidly with time. Since heat flow through convection at the surface is much faster than heat flow by conduction inside the ice cream, heat near the surface is depleted by convection after a short period of time in hardening. After the initial burst of cooling, the low conductivity of ice cream becomes the limiting factor, and a large convective coefficient helps little.

The ice cream will eventually approach the air temperature if it resides in the hardening room long enough. In manufacturing, however, time is always an important factor. For

hardening, a longer residence time also means higher energy consumption. An appropriate condition under which the hardening is deemed accomplished needed to be established. In this work, when the warmest point in the ice cream reaches -15^{o}C, hardening is considered finished. The time required for this is referred to here as the hardening residence time and denoted by t_{-15C}. The residence time provides a basis for determining the efficiency of the hardening process.

To reach a bottom-center (warmest point) temperature of θ= 0.68 (-15^{o}C), Model 2.3 required 7020 sec (1.95 hr), 5148 sec (1.43hr), and 4860 sec (1.35 hr) for coefficients of h = 30, 210, and 630 W/(m^2·K), respectively. To investigate how residence time t_{-15C} changes with the convective coefficient, the model was rerun using a wider range of convective coefficients including 1, 3, 6, 10, 30, 60, 100, 210 and 630 W/(m^2·K). Figure 2.9 shows the variation of residence time t_{-15C} versus the convective coefficient h (the middle grey solid line labeled -6^{o}C).

The draw temperature is the temperature of the ice cream when exiting the freezer, which is consequently the initial hardening temperature. The effect of the draw temperature on hardening time was achieved by changing its initial temperature for the transient analysis. The initial temperature of the base Model 2.3 was changed from -6^{o}C to -2,-4,-8 and -10^{o}C. The results, presented in Figure 2.9, show an interesting trend. When the initial temperature was lowered by 4^{o}C over all convective coefficients studied it resulted in t_{-15C} being reduced by 40% on average. The trend is seen through the -2^{o}C to -6^{o}C draw temperature data which had a 39% difference and for -6^{o}C to -10^{o}C draw temperature data which had a 40.8% difference. It is reasonable to conclude that decreasing draw temperature will reduce hardening energy significantly when only the hardening process is considered.

All five curves in Figure 2.9 share one common characteristic: at small *h*, t_{-15C} decreases rapidly with increasing *h*; after a certain value, however, further increase in *h* has little impact on t_{-15C}. The phenomenon can be explained in light of competition in heat transfer between convection and conduction. At small *h*, heat flow from the inside of the ice cream to the surface by conduction is faster relative to convection, and consequently convective heat transfer at the surface is the bottleneck of the process. This leads to convection-control. At large *h*, convective heat transfer at the surface is faster relative to conduction, and conduction from the inside to the surface becomes the bottleneck of the process, leading to conduction-control. The concept of *convection-conduction control transition* (*CCCT*) is hereby proposed which signifies the transition from convection to conduction control. For convenience, the convective coefficient at *CCCT* is denoted here as h_{CCCT}. When *h* is less than h_{CCCT}, increasing air velocity, which in turn increases h, significantly accelerates heat transfer and hence reduces hardening residence time. But when *h* is greater than h_{CCCT}, increasing air velocity does not have a significant impact on residence time since heat transfer is predominantly limited by conduction inside the ice cream. As shown in Figure 2.9, *CCCT* corresponds to the "knee" region of the curve, and h_{CCCT} is in the range of 30 to 100 W/(m^2·K). Since the body size affects transient heat transfer, the Biot number, defined by

$$Bi = \frac{hL_C}{k} \tag{2.3}$$

where L_C is the characteristic length (Incropera et al., 2007), is a more appropriate parameter to indicate *CCCT*. As the characteristic length for the sqround, L_C, commonly defined as the ratio

of volume to surface area, is about 20 mm for the sqround geometry, and the average conductivity for ice cream from -6 to -15 ^{o}C is about 0.4 W/(m·K), the Biot number for *CCCT*, denoted as Bi_{CCCT}, is about 1.5 to 5. It is worth noting that CCCT is not a well defined point but rather a gradual transition, and therefore the value of 1.5 to 5 for Bi_{CCCT} should be used only as an indicator, rather than a precisely defined value.

3.1.4 Results for Models 2.4 and 2.5

The purpose of Models 2.4 and 2.5 was to investigate how hardening residence time would be affected if convection was allowed by cutting a hole in the center of the sqround. The transient temperature distribution at 1 hr for Model 2.5 is shown in Figure 2.10. The figure shows that the hole has moved the warmest point from the bottom center to an area in the mid section of the sqround. The data shows that for *h* from 10 to 210 W/(m^2·K), the average time saved was 47% for Model 2.4 (Hole 1) and 58% for Model 2.5 (Hole 2). The knee shape of the three response curves is similar to that of Figure 2.9, reaffirming the convection-conduction control transition.

3.1.5 Results for Models 2.6 and 2.7

Slicing the volume into separate parts for the hardening process was investigated through Models 2.6 and 2.7. Ice cream is insulatory, so reducing the thickness leads to faster cooling. The models showed that hardening a sqround in 4 pieces dramatically reduces the overall time in comparison with hardening the whole volume.

The percentage of time saved with Models 2.4-2.7 is shown in Figure 2.11. For *h* of 30 W/(m^2·K), Model 2.7 had a 63.1% decrease in residence time compared with the base Model 2.3, Model 2.5 had a 54.6% decrease, Model 2.4 had a 44.2% decrease, and Model 2.6 had a 25.9%

decrease. It was found that slicing the volume into 4 pieces was the best option in this study for saving time and energy in the hardening process.

3.2 Discussion

Feasibility of modeling ice cream hardening with a homogeneous, solid material. Comparisons with Tracey and McCown's (1934) experiments show that ice cream hardening can be modeled with reasonable accuracy using a homogeneous solid material with temperature dependent properties. Discrepancies between the current FEA models and experiments are generally within 10%. It should also be noted that although the solid model captures heat transfer in ice cream hardening satisfactorily, it lacks the ability to capture explicit phase change and other important microstructural changes during hardening.

Effects of boundary conditions on hardening residence time and energy usage. Convection is the primary mode of heat transfer during the process. An increase in air velocity will lead to an increase in convective heat transfer, which will result in a shortened hardening time. However, the rate of reduction in residence time depends on operational conditions. When the convective coefficient h is less than h_{CCCT}, increasing h by increasing air velocity decreases residence time appreciably. When the convective coefficient h is greater than h_{CCCT}, increasing h does not have a significant impact on residence time since heat transfer is limited by conduction inside the ice cream. A shorter residence time saves manufacturing time which may result in energy savings, but increasing the convective coefficient requires more energy. This indicates that energy consumption for operating the hardening chamber must be known to predict net energy savings. Since increasing h above h_{CCCT} has small effect on shortening residence time, it can be concluded that the optimal convective coefficient should not exceed h_{CCCT}.

Effects of shape and size on residence time and energy usage. In general, smaller sizes result in shorter residence times, and package shapes that have a larger surface to volume ratio also help reduce residence times. Producing small size packages for hardening and packing them into larger sizes after hardening is one way to reduce residence time and save energy.

Optimal hardening condition. The simulation shows that the convection-conduction control transition, h_{CCCT}, is characterized by a Biot number ranging from 1.5 to 5. This provides a simple way to estimate the optimal hardening condition. For example, for a cubic gallon of ice cream, with an average thermal conductivity of 0.4 W/(m·K) and an L_C of 26 mm, h_{CCCT} turns out to be in the range of 23 to 77 W/(m^2·K). Typical conditions of 30 to 60 W/(m^2·K) coincide with the predicted transition. Further increase in h beyond the convection-conduction control transition escalates energy consumption but does not have a significant impact on the residence time. A smaller package size decreases the characteristic length L_C and leads to a smaller optimal heat transfer coefficient h_{CCCT}.

4. Conclusions

Industrial ice cream production encompasses a number of processes to create a product with desirable qualities. The hardening process has a significant impact on the quality of the final product. In this work, finite element models were used to investigate the hardening process. Temperature dependent properties were retrieved from the literature. FEM results were compared with previously published experimental data (Tracy and McCown, 1934). The comparison validated the FEA models.

The study quantifies conditions for optimal energy efficiency for ice cream hardening. The coefficient for convection-conduction control transition, h_{CCCT}, is characterized by a Biot number in the range of 1.5 to 5. For a gallon of typical ice cream, h_{CCCT} is 23 to 77 W/(m^2·K). Increasing the convective coefficient up to h_{CCCT} by increasing air flow or decreasing air temperature shortens the residence time significantly. Values beyond h_{CCCT} do not have a significant impact on the residence time. This work also demonstrates the design capability of the models to optimize energy usage in the hardening process.

Draw temperature has a significant impact on hardening time and can reduce residence time by 40% for every 4^{o}C dropped. Hardening a given volume with a central hole can lead to significant energy savings as it reduces residence time by up to 50%. Furthermore, slicing a volume into separate sections is also a promising way to decrease hardening time.

References for Chapter 2

Adapa S, Schmidt KA, Jeon IJ, Herald TJ, Flores RA. 2000. Mechanisms of ice crystallization and recrystallization in ice cream: a review. Food Rev Int 16:259–71.

Aldazabal J, Martin-Meizoso A, Martinez-Esnaola JM, Farr R. 2006. Deterministic model for ice cream solidification. Comp Mat Sci 38:9-21.

Aleong JM, Frochot S, Goff HD. 2008. Ice recrystallization inhibition in ice cream by propylene glycol monostearate. J Food Sci 73:463–8.

Ben-Yoseph E, Hartel RW. 1998. Computer simulation of ice recrystallization in ice cream during storage. J Food Eng 38:309-29.

Bolliger S, Kornbrust B, Goff HD, Tharp BW, Windhab EJ. 2000. Influence of emulsifiers on ice cream produced by conventional freezing and low-temperature extrusion processing. Int Dairy J 10:497–504.

Cindio DB, Iorio G, Romano V. 1985. Thermal analysis of the freezing of ice cream brickettes by the Finite Element Method. J Food Sci 50:1463–6.

Clarke C. 2004. The Science of Ice Cream. Cambridge, UK: Royal Society of Chemistry.

Cogne C, Andrieu J, Laurent P, Besson A, Nocquet J. 2003. Experimental data and modelling of thermal properties of ice creams. J Food Eng 58:331-41.

Cordell JM, Webb DC. 1985. The freezing of ice cream. Proceedings of the Int Symp Heat and Mass Transfer Prob in Food Eng [Accessed in: Thermal analysis of the freezing of ice cream brickettes by the Finite Element Method; de Cindio et al. (1985)]; 1972 October 24-27; Wageningen, NL. J Food Sci 50:1464.

Donhowe DP, Hartel RW, Bradley RL Jr. 1991. Determination of ice crystal size distributions in frozen desserts. J Dairy Sci 74:3334-44.

Donhowe DP, Hartel RW. 1996. Recrystallisation of ice cream during controlled accelerated storage. Int Dairy J 6:1191-208.

Fellows PJ. 2000. Food Processing Technology Principles and Practices. 2nd ed. New York: CRC Press.

Fennema OR, Powrie WD, Marth EH. 1973. Low-temperature Preservation of Foods and Living Matter. New York: Marcel Dekker.

Flores AA, Goff HD. 1999. Ice crystal size distributions in dynamically frozen model solutions

and ice cream as affected by stabilizers. J Dairy Sci 82:1399-407.

Food Processing Equipment [Internet]. 2009 [Accessed 2009 November 1]. Available from: http://food-processing-equipment.biz.

Greener RC. 2010. Rapid hardening systems [Accessed 2009 Dec 1]. Available form: http://www.freestech.com/img/Hardening%20And%20Storage%20Lecture2009.ppt

Higgins KT. 2009. Get smart about energy usage. Food Eng Magazine. 2009. Available from: http://www.foodengineeringmag.com.

IDFA. Dairy Facts. 2009 ed. International Dairy Foods Association. Washington DC.

Incropera FP, DeWitt DP, Bergman TL, Lavine, AS. 2007. Fundamentals of Heat and Mass Transfer. 6th ed. New Jersey: Wiley and Sons.

Marshall RT, Goff HD, Hartel RW. 2003. Ice Cream. 6th ed. New York: Kluwer Academic/Plenum Publishers.

Russell AB, Cheney PE, Wantling SD. 1999. Influence of freezing conditions on ice crystallization in ice cream. J Food Eng 39:179–91.

Schmidt KA. 2004. Dairy: Ice Cream. In: Smith JS, Hui YH, editors. Food Processing Principles and Applications.1st ed. Iowa: Blackwell Publishing.

SolidWorks [Internet]. 2010. [Accessed 2010 Feb 1]. Concord, MA: Dassault Systemes SolidWorks Corp. Available from: SolidWorks.com.

Sutton R, Bracey J. 1996. The blast factor. Dairy Industries Int 61:31-3.

Tracey PH, McCown CY. 1934. A study of factors related to the hardening of ice cream. J Dairy Sci 17:47-60.

U.S. Energy Information Administration [Internet]. 2006 Energy consumption by manufacturers – data tables [Accessed 2009 Oct 1]. Available from: http://www.eia.doe.gov/emeu/mecs/contents.html.

Zuritz CA, Singh RP. 1985. Modelling temperature fluctuations in stored frozen food. Int J Refrig 8:289-93.

Nomenclature for Chapter 2

Parameter	Meaning	Value used
A_c	Cross section of the channel, m^2	0.1329
C_p	Specific heat capacity, J/(kg·K)	500
D_H	Hydraulic diameter, m	0.1284
E_m	Lower reference energy, kW·hr	
E_n	Higher reference energy, kW·hr	
F_o	Fourier number	≤ 0.25
h	Convective heat transfer coefficient, W/(m^2·K)	30; 60; 210; 630
h_{CCCT}	h at convection-conduction control transition	
h_m	Lower reference heat transfer coefficient, W/(m^2·K)	30
h_n	Higher reference heat transfer coefficient, W/(m^2·K)	210; 630
H_1	Approximate height of ice cream package, m	0.10
H_2	Vertical clearance between conveyor belts, m	0.1113
k_f	Thermal conductivity of fluid, W/(m·K)	0.0223
L	Length in depth dimension of the channel, m	0.0633
$\overline{Nu}_D$	Average Nusselt number	≥131.3
$Nu_{D,fd}$	Nusselt number for fully developed region	131.3
Pr	Prandtl number	0.720
P_w	Wetted perimeter of the channel, m	1.039
q_t	Heat transfer rate at a given time step, W	
Q_t	Total heat transferred up to a given time step, kW·hr	
R_{e_D}	Reynolds number	5.61×10^4
t_m	Lower reference time, hr	1.58
t_n	Higher reference time, hr	1.18; 1.13
T_i	Initial ice cream temperature, °C	-6 (= 267 K) (de Cindio et al. 1985)
T_∞	Air temperature, °C	-34 (= 239 K) (de Cindio et al. 1985)
T_f	Final surface temperature of ice cream container, K	255
T_s	Average surface temperature of ice cream container, K	261
T_m	Mean temperature for determining fluid properties, K	250
V_∞	Air velocity, m/s	5 m/s, into page (Fellows 2000)
W_1	Approximate width of ice cream package, m	0.12
W_2	Distance between conveyor brackets, m	0.4064
ν_f	Kinematic viscosity of fluid, m^2/s	$11.44\times10^{-6}\,m^2\cdot s^{-1}$
ρ	Mass Density, kg/m^3	500

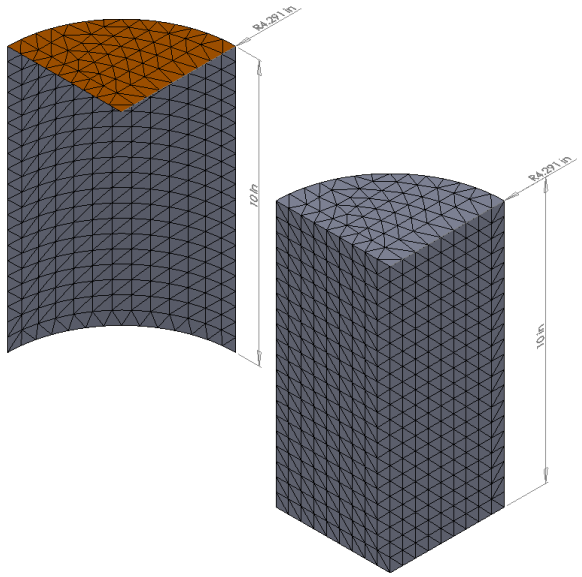

Figure 2.1 Model 2.2

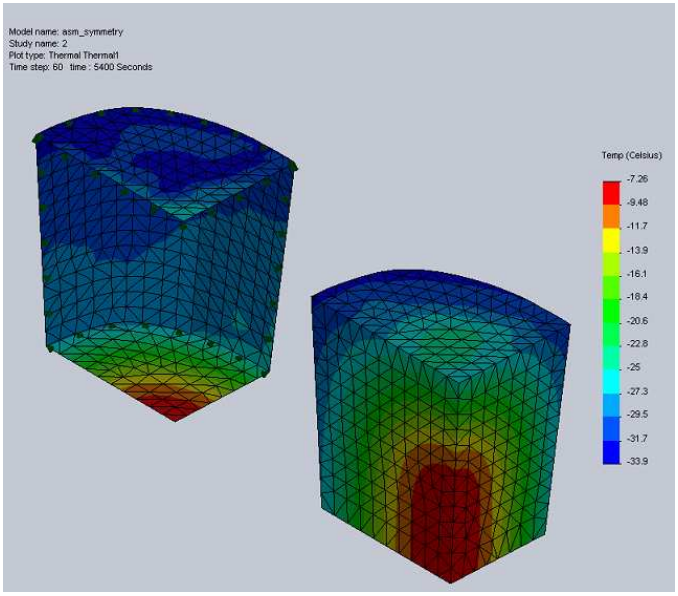

Figure 2.2 Model 2.3 Temperature Distribution

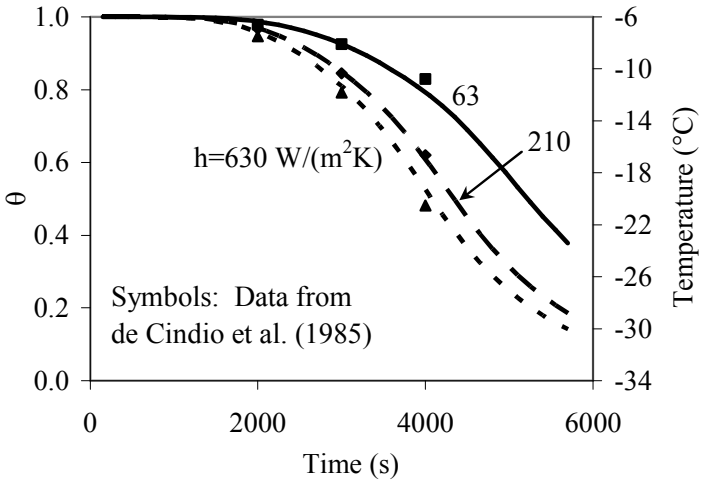

Figure 2.3 Model 2.1 Temperature Variations

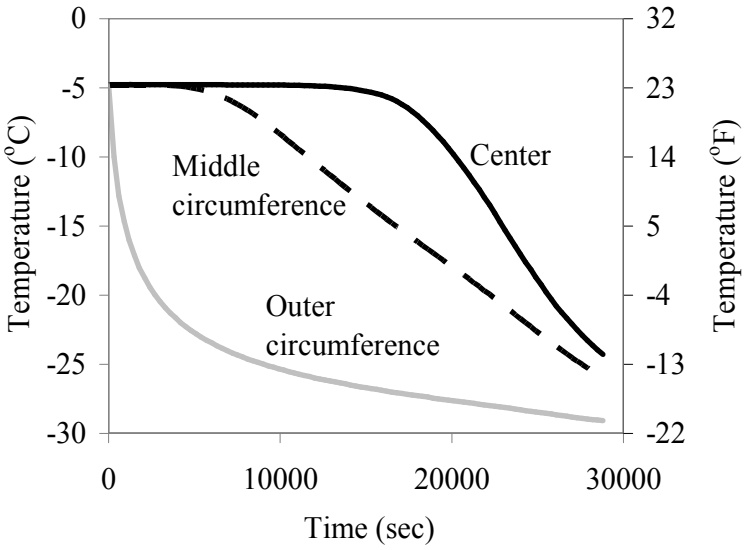

Figure 2.4 Temperature variation at three locations for Model 2.2.

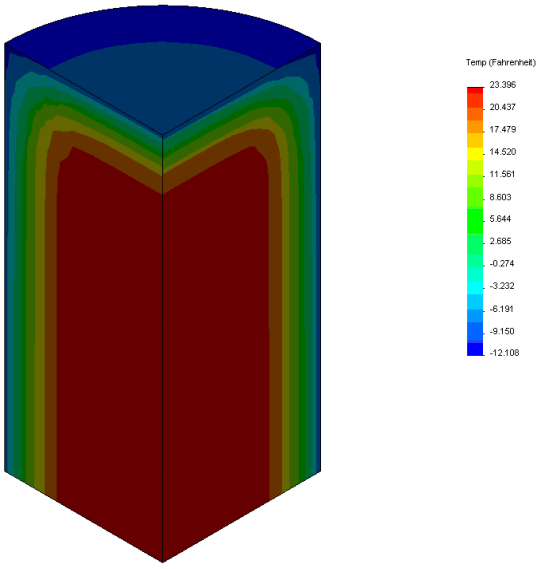

Figure 2.5 Model 2.2 Temperature Distribution at 3900 sec (1 hr, 5 min).

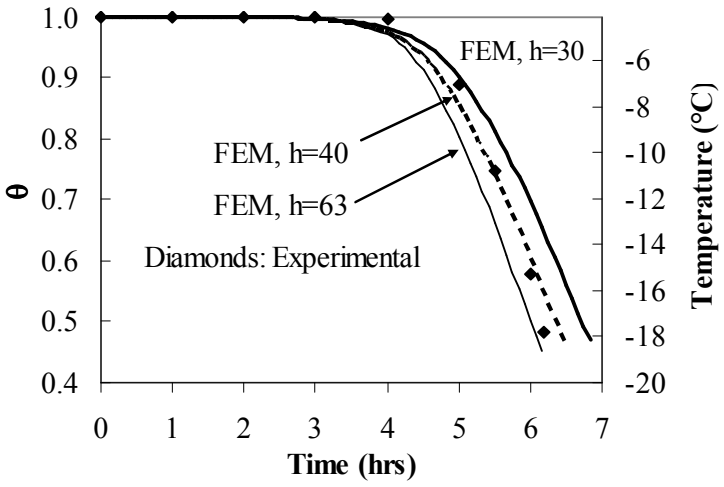

Figure 2.6 Model 2.2 Results with Experimental Comparison.

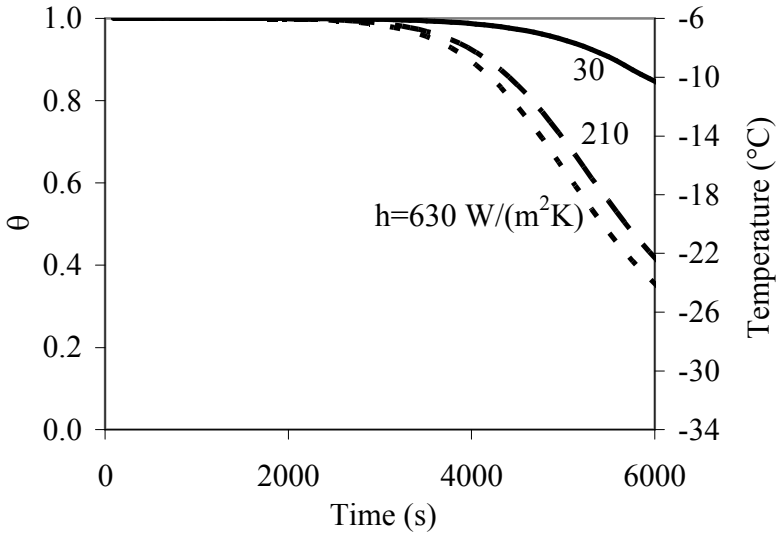

Figure 2.7 Model 2.3 Mid-Center Temperature Variation.

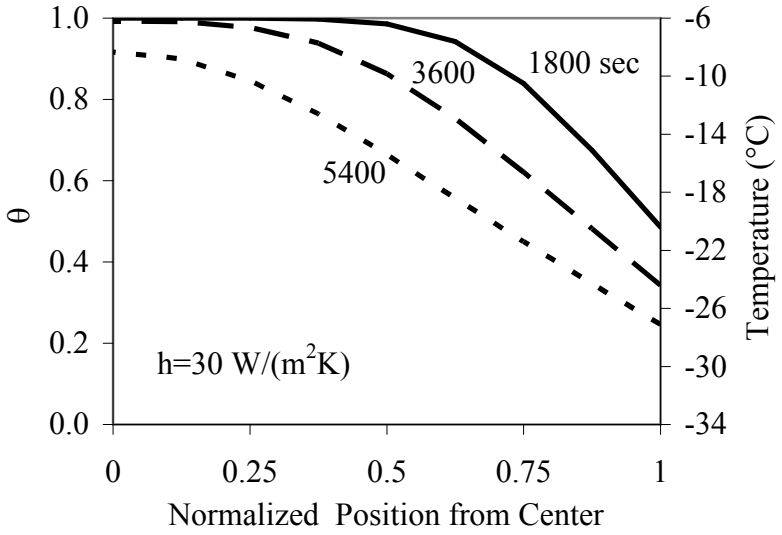

Figure 2.8 Transient response of horizontal temperature distribution from center to outer surface from Model 2.3 with a convective coefficient of 30 W/(m^2•K).

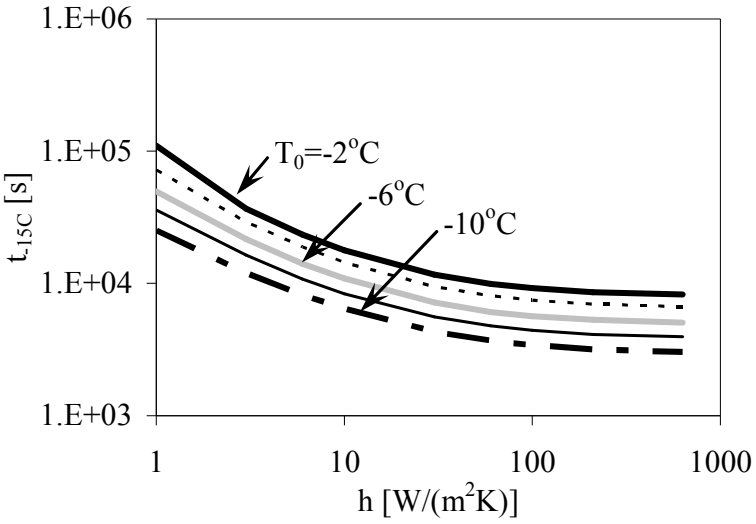

Figure 2.9 Variation of residence time versus the convective coefficient *h* for draw temperatures of -10,-8,-6,-4 and -2°C from Model 2.3.

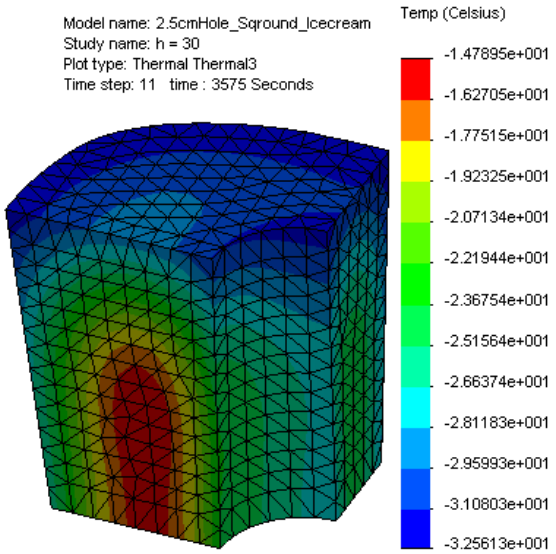

Figure 2.10 Transient temperature distribution at 1 hr for Model 2.5.

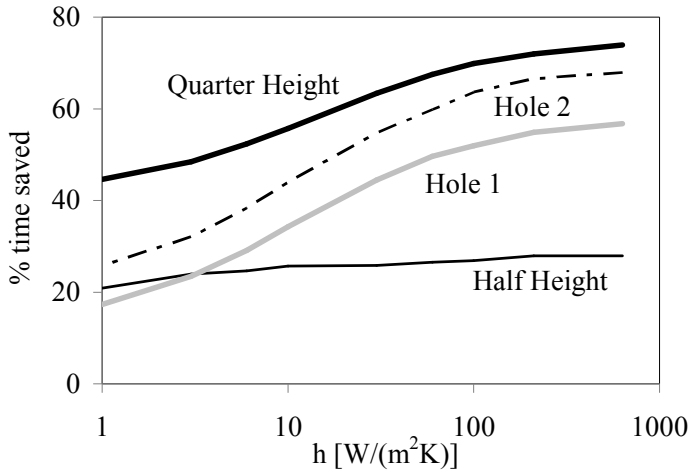

Figure 2.11 Percent time saved for Models 2.4-2.7 compared to Model 2.3.

Table 2.1 Ice Cream Material Properties (Cogne et al. 2003; Cordell and Webb 1985)

Ice Cream Material Properties	
Mass Density	ρ (kg/m^3)
Constant	500
Thermal Conductivity	
Temperature Dependent: T (°C)	k (W/(m*K))
-25	0.48
-20	0.46
-15	0.44
-10	0.41
-5	0.35
0	0.2
Specific Heat Capacity	
Temperature Dependent: T (°C)	Cp (J/(kg*K))
-30	2100
-25	2300
-20	3000
-15	4700
-9.5	9000
-7	13000
-6	17000
-5.5	21500

Table 2.2 Material Properties of Container (Incropera et al. 2007)

Mass Density *Constant*	ρ (kg/m^3) 930
Thermal Conductivity Constant	k (W/(m·K)) 0.18
Specific Heat Capacity *Constant*	Cp (J/(kg·K)) 1340

Table 2.3 Geometric Properties of Sqround Container

Major Diameter of Top Surface (mm)	172.96
Minor Diameter of Top Surface (mm)	130.99
Major Diameter of Bottom Surface (mm)	150.51
Minor Diameter of Bottom Surface (mm)	108.52
Height (mm)	98
Draft Angle (Degrees)	5.46
Wall Thickness (mm)	1
Volume Capacity (L)	1.66

Chapter 3 - Population Balance Model for Ice Cream Hardening

Abstract

A three-dimensional population balance model (PBM) is constructed for the simulation of ice crystal nucleation and growth in the ice cream hardening process. Microstructural characteristics are achieved through a three-part model development: (1) a single-phase cylinder with temperature-dependent material properties is validated with previous experimental data, (2) the single-phase material is reconfigured into a cube, and (3) the cubical model is then advanced to a multiphase PBM approach. The final crystallization results are verified with previous experimental research. The work provides a flexible and efficient approach to predict the ice crystal size distribution (CSD) of ice cream following the hardening process. The computational method is applicable for myriad food-freezing processes, alloy solidification, and other multiphase systems.

1. Introduction

Ice cream manufacturing requires numerous carefully-controlled processes to yield a high quality final product (Marshall et al., 2003). While each individual step is required to achieve this goal, the freezing and hardening processes have the greatest impact on the ice cream microstructure and therefore the resulting texture quality. Substantial research has been conducted in this field, but much uncertainty remains due to the inherent complexity of the crystallization kinetics (Cook and Hartel, 2010). Most ice crystallization studies have focused on experimental investigation, rather than computational modeling. Experimental examples include

an extensive study by Russell et al. (1999) to determine the most dominant crystallization mechanisms within a scraped surface heat exchanger (SSHE). They also briefly considered the conventional hardening process. Adapa et al. (2000) reviewed the influence of fat content and fat replacers on the viscoelastic properties of ice cream. Crilly et al. (2008), as well as Regand and Goff (2005), studied the effects of ice structuring proteins (ISPs). Other innovations include the low temperature extrusion (LTE) process detailed by Wildmoser et al. (2004). Their work showed that the twin screw extrusion system (TS-LTE) resulted in significant quality improvements over the conventional SSHE / hardening combination. As reviewed by Zheng and Sun (2006), ultrasound vibrations have been used to break up ice crystals during food freezing processes, including ice cream.

In contrast to the quickly developing experimental research, ice cream freezing and hardening simulations are fewer in number. Computational examples include a two-dimensional FEA study by de Cindio et al. (1985), which considered hardening of ice cream as a homogeneous single phase solid material. Rauth et al. (2010) used a three-dimensional FEA model to replicate the experimental hardening results presented by Tracey and McCown (1934). Cromer et al. (2010) studied energy efficiency in the hardening process by varying package configurations. Aldazabal et al. (2006) performed a hardening simulation in which sugar diffusion and ice crystal microstructure were modeled. Ben-Yoseph and Hartel (1998) simulated recrystallization during ice cream storage. A popular approach for simulating particulate processes is through the use of the population balance equations (PBE) presented by Hulburt and Katz (1964) and refined for continuous crystallization by Randolph and Larson (1988). Some researchers have combined PBE with computational fluid dynamics (CFD) to model dynamic crystallization processes. Woo et al. (2006) modeled antisolvent crystallization in an agitated

semibatch vessel using combined CFD-PBE. Similarly, Lian et al. (1988) simulated the crystallization of a sucrose solution within an SSHE using this method.

In this work, a three-dimensional population balance model (PBM) is constructed for the simulation of ice crystal nucleation and growth in the ice cream hardening process. The crystalline microstructure is rendered through the following three-part model development. (1) A single-phase cylinder with temperature-dependent material properties is compared with previous experimental results to verify the accuracy of the heat transfer model. (2) Next, the single-phase material is reconfigured into a cube to bridge to previous empirical crystallization data. (3) The cubical model is then advanced to a multiphase PBM approach to simulate the crystal size distribution (CSD). The final crystallization results are verified with previous experimental research. The work provides a flexible and efficient approach to predict the CSD throughout the ice cream hardening process. The computational method is applicable for myriad food-freezing processes, alloy solidification, and other multiphase systems.

2. Materials and Methods

2.1 Theory

This section outlines the underlying theory and equations that characterize heat transfer for all three models as well as crystallization for the multiphase model. Assumptions are provided in this section, and computational-specific details are presented in Section 2.2.

2.1.1 Model 3.1: Single Phase Cylindrical

The ice cream hardening process was modeled by starting with a homogeneous single phase material (ice cream mix), and then advancing the approach to explicitly include phase change and crystal growth. The term "explicitly" refers to the fact that in the multiphase model, ice is modeled explicitly as a separate phase. In the single phase model, phase change is not modeled explicitly but captured through temperature dependent properties of real ice cream material. Thus the Model 3.1 approach is considered "implicit." The following assumptions were made for Model 3.1:

1. Air velocity in the hardening chamber, air temperature, and convective heat transfer coefficient (*HTC*) are constant. An example *HTC* calculation is provided in Appendix B.
2. Internal flow is negligible during blast freezer hardening. This precludes the need for momentum calculations.
3. The material is isotropic, and phase change is modeled implicitly through temperature dependent properties. Additional details are available in Section 2.2.1.
4. The cylindrical geometry of the ice cream is simplified through the use of an axisymmetric mesh. Moreover, the height dimension is also symmetric. This allows for half the height to be modeled, with the symmetric boundary maintained as adiabatic.

With these assumptions, the following governing equation characterizes heat transfer in a single phase material:

$$k(T)\left[\frac{\partial^2 T}{\partial x^2}+\frac{\partial^2 T}{\partial y^2}+\frac{\partial^2 T}{\partial z^2}\right]-\rho C_p(T)\frac{\partial T}{\partial t}=0 \qquad (3.1)$$

where x, y, and z are the Cartesian coordinates, t is time, T is the temperature which changes with position and time, i.e., $T = T(x, y, z; t)$, $k(T)$ is the temperature dependent thermal conductivity, ρ is the mass density, and $C_p(T)$ is the temperature dependent specific heat capacity. The equation can be solved by considering the initial and boundary conditions. In this study convective and adiabatic boundary conditions were modeled.

2.1.2 Model 3.2: Single Phase Cubical and Model 3.3: Multiphase Cubical

Model 3.1 was useful as it gave experimental validation for using the single phase material. This verification allowed for the single phase material to be employed by Model 3.2, which was a single phase, cubical model. As the only parameter changed between Models 3.1 and 3.2 was the geometry, results from Model 3.2 were used as a benchmark for Model 3.3. The third model employed a multiphase cubical geometry. The primary phase was the ice cream mix used for Models 3.1 and 3.2, while the secondary phase was pure ice. Mass transfer between these phases is described in Section 2.2.2. Assumptions for Model 3.2 were the same as Model 3.1. Assumptions for Model 3.3 are provided below.

1. As with the previous models, air velocity, air temperature, and convective *HTC* are constant. An example *HTC* calculation is provided in Appendix B.
2. Internal flow is negligible during blast freezer hardening. Again, this precludes the need for flow calculations.

3. The primary phase (ice cream mix) has the same properties as the material used for Models 3.1 and 3.2. The secondary phase (pure ice) is generated by transferring mass from the primary phase. This is governed by the user defined functions (UDFs) provided in Section 2.2.2.
4. One-eighth of the cube is modeled to utilize problem symmetry.
5. Only primary nucleation and growth are considered.
6. Ice crystals are circular. The term "crystal length" refers to diameter.

With these assumptions, Equation 3.1 was solved on a multiphase basis. These calculations were iteratively alternated with PBE. This was a combined theoretical and empirical approach in which the crystal nucleation and growth terms are handled by UDFs. The method has many similarities with the work of Lian et al. (2006). But, their study involved a pure sucrose solution in a continuous freezer, whereas in this study the parameters differed as the material was an ice cream mixture. Moreover, the process studied was hardening. This step involves blowing cold air (roughly -30°C) across the product to solidify and preserve it.

Three techniques are available using the PBM of Fluent 6.3 (2006): Discrete, Standard Moment, and Quadrature Moment. Crystallization in this simulation was carried out using the Discrete Method of PBE developed by Hounslow (1988), Litster (1995), and Ramkrishna (2000). This approach allows for the crystal size distribution (CSD) to be computed directly. It is especially useful when the range of crystal sizes is known *a priori* (Fluent 6.3, 2006). The PB equation that governs ice crystallization is as follows.

$$\frac{\partial}{\partial t}\left[n(V,t)\right]+\nabla\cdot\left[\vec{u}n(V,t)\right]+\nabla_V\cdot\left[G_V n(V,t)\right]=B_{ag}+B_{br}-D_{ag}-D_{br} \tag{3.2}$$

Here n(V,t) refers to crystal density (#·m^{-3}) as a function of crystal volume (V) and time (t). $\nabla \cdot \left[\vec{u} n(V,t)\right]$ refers to crystal flow through the control volume, which is zero due to Assumption 2. $\nabla_V \cdot \left[G_V n(V,t)\right]$ represents volumetric crystal growth. B refers to crystal birth, D refers to crystal death, and the subscripts *ag* and *br* refer to aggregation and breakage. Aggregation and breakage are not considered here, therefore the right-hand side of Equation 3.2 is zero. Equation 3.2 is subject to the boundary and initial conditions given by Equations 3.3 and 3.4 below.

$$n(V, t=0) = n_V \tag{3.3}$$

$$G_V n(V=0, t) = \dot{n}_0 \tag{3.4}$$

Specific values of these parameters are provided in the Simulation Section. When cell conditions were appropriate, as described in Section 2.2.2, ice crystals proceeded to nucleate and grow. This mass was transferred from the primary phase to the secondary. Heat transfer equations were solved for the effective composite material. Its behavior was similar to the single phase material. The crystallization results from Model 3.3 were compared with the previously published experimental data of Russell et al. (1999).

2.2 Simulation

2.2.1 Model 3.1: Single Phase Cylindrical

The first simulation modeled an experimental study by Tracey and McCown (1934). In their work, the temperature histories of ice cream volumes placed in a conventional hardening room were measured and recorded. Copper-constantan thermocouples, which were accurate to within 0.06°C (0.1°F), were used to measure temperature changes at selected surface, interior, and center points. The following simulation corresponds to Figure 6 from Tracey and McCown (1934); forced convective cooling of 19 L (5 gal) cylindrical cans of ice cream at -30°C (-22°F). The height of each can was 50.8 cm (20 in), which corresponded to a radius of 10.9 cm (4.29 in). For the current model, an axisymmetric mesh approach was taken to utilize the inherent symmetry of the analysis. Moreover, the top and base of the cylinder were assumed to share equal convective boundary conditions, thus only half the height needed to be modeled. The symmetric base was maintained as adiabatic to enforce the height-symmetric boundary condition. The height of the symmetric (reduced) model was 25.4 cm (10 in). Figure 3.1 shows the domain of simulation and boundary conditions. Note that the container layer was not included since it was a thin layer of steel, and its thermal resistivity was negligible compared to the relatively large and insulatory ice cream volume. The commercial CFD software Fluent 6.3 (2006) was used to model the heat transfer, but flow calculations were not needed since the ice cream was assumed to be internally static. The ice cream initial temperature was -4.78°C (-23.4°F). Hardening residence or dwell time was defined from the start of the hardening process until the temperature at the warmest point of the ice cream (base-center of the symmetric model) decreased to at least -18°C. Convective conditions were maintained at the outer faces (line segments for the axisymmetric plane). Convective heat transfer coefficients of 30 and 40 $W \cdot m^{-2} \cdot K^{-1}$ were used in two separate studies, and a bulk ambient air temperature of -30°C was enforced. The first *HTC* was calculated using correlation equations from Incropera et al. (2007),

and the second value of the *HTC* was used to fit the experimental temperature history more closely. These values compare reasonably well with the range given by Fellows (2000) of 25~30 $W \cdot m^{-2} \cdot K^{-1}$. An example *HTC* calculation is provided in Appendix B.

Other model details include geometry creation and mesh generation, each of which was performed using Gambit 2.4.6 (Fluent 6.3, 2006). Both the height and radial dimensions were divided into ten segments using quad-elements. Subsequent studies were run using finer and coarser meshes to ensure convergence. The initial time step was determined using the Fourier Number, and was varied similarly with the mesh to ensure numerical accuracy. Details of the Fourier Number can be found elsewhere (Incropera et al., 2007). The calculation resulted in a critical time step of 5 min. A total of 7 hrs (84 time steps) was simulated. Material properties for the simulation were obtained from data in the literature. Specifically, density was from de Cindio et al. (1985), thermal conductivity was from Cogne et al. (2003), and specific heat capacity was from Cordell and Webb (1972). Table 2.1 shows the values that were used for these properties. Note that the thermal conductivity and specific heat capacity are directly related to the ice content. As the liquid to solid water (ice) phase change occurs, the specific heat capacity spikes to account for the latent heat of fusion. This is how the single phase material was used to accurately model the complex ice cream mix.

2.2.2 Model 3.2: Single Phase Cubical and Model 3.3: Multiphase Cubical

Model 3.1 was useful for validating the single phase (ice cream) properties with actual experimental data. The modeling approach was then refined by explicitly considering the ice phase changes that take place during the ice cream hardening process. This was achieved by modeling certain parameters of the experimental study presented by Russell et al. (1999). Their

focus was primarily on the crystallization kinetics within an SSHE, but hardening was also considered. The study consisted of a 0.5 L (1.06 pt), cubical ice cream volume hardened in a conventional blast freezer. This volume corresponds to cube side lengths of 7.937 cm. One-eighth of the cube was modeled to utilize symmetry, thus side lengths of 3.969 cm were used for the symmetric (reduced) model. Figure 3.2 shows parameters for the cubical models. The temperature distribution is also shown for Model 3.2 at 20 min of dwell time in the freezer. Certain characteristics of the ice cream mixture and experimentation varied from the Tracey and McCown (1934) study, but conditions were similar enough that the same computational setup could be used for comparison. These details have been presented in Section 2.1. For Models 3.2 and 3.3, the ice cream initial temperature was -4.1°C. A 5 min time step was used again, but this time only 1 hr (12 time steps) was required to achieve a warmest point temperature of -18°C. This is a result of the fact that the cubical ice cream volume was much smaller than the cylindrical configuration.

After the single phase baseline was established using Model 3.2, PBE calculations were performed using Model 3.3. Fluent's Eulerian Multiphase Model (Fluent 6.3, 2006) was used to simulate the composition changes in the mixture. Mass transfer from the primary to the secondary phase was handled by the discrete population balance model, as described in Section 2.1.2. PBE proceeded using power laws of ice volume fraction within UDFs. Equation 3.5, below, was used to calculate the "freezing temperature" (T_f) of a given cell. Note that T_f given by Equation 3.5 is an empirical parameter rather than the actual freezing point depression value (Lian et al., 2006). Equation 3.6, also below, was used to calculate the equilibrium ice content (θ_e) for temperatures below T_f. This was determined for initial sucrose concentrations (c_0) of 0.25 and 0.15, as explained in the following sections.

$$T_f = \frac{5c_0}{c_0 - 0.85} \tag{3.5}$$

$$\theta_e = 1 - c_0\left(\frac{T_f - 5}{0.85T_f}\right) \tag{3.6}$$

Equations 3.5 and 3.6 correspond to an empirically-determined relationship from Lian et al. (2006). The material of that study was different, but the general crystallization kinetics proved to be similar enough to capture the ice cream hardening behavior. Model parameters were fit to the experimental ice cream hardening data (Russell et al., 1999).

Equilibrium ice content was calculated using an initial sucrose concentration (c_0) of 0.25 by weight, which corresponds to T_f of -2.1°C. These parameters were used to determine the nucleation and growth constants; k_b and k_g, as well as the power indices; n_b and n_g. The value for k_b was set at 8.0e5 #·m^{-3}·s^{-1}, and n_b was 100. A value of 6.0e-9 m·s^{-1} was used for k_g, and n_g was 1.0e-6. Equations 3.7 and 3.8 below show how the nucleation ($\dot{n}_0$) and growth (G_L) terms were calculated. Note that G_L refers to crystal growth based on length, and θ_i is the ice fraction at a given time step.

$$\dot{n}_0 = k_b\left(1 - \frac{\theta_i}{\theta_e}\right)^{n_b} \tag{3.7}$$

$$G_L = k_g\left(1 - \frac{\theta_i}{\theta_e}\right)^{n_g} \tag{3.8}$$

Together these equations enabled the multiphase model to calculate the ice cream CSD throughout the hardening process. Heat transfer and PBE were solved in a continuously alternating iterative approach.

3. Results and Discussion

For conciseness, the dimensionless temperature θ is defined as:

$$\theta = \frac{T_t - T_\infty}{T_i - T_\infty} \tag{3.9}$$

where T_t is the ice cream temperature at a given time, T_∞ is the bulk ambient temperature, and T_i is the initial ice cream temperature.

3.1 Model 3.1: Single Phase Cylindrical

The homogeneous single phase material was shown to capture the thermal response of the ice cream quite well. Figure 3.1 shows the temperature contours of the cylinder at 6 hrs and 50 min. At that point, all of the ice cream had dropped below the required -18°C. The experimental study of Tracey and McCown (1934) took approximately 4 hrs for the center temperature to begin changing noticeably and 6.2 hrs for the center temperature to reach -18°C (θ = 0.48). The numerical model presented here had slightly different curves. For an *HTC* of 30 $W \cdot m^{-2} \cdot K^{-1}$, approximately 3.6 hrs were required for the center to begin changing, and about 6.7 hrs were necessary for the center temperature to reach -18°C (θ = 0.48). Figure 3.3 shows a

direct comparison of the experimental and numerical results. Simulated curves for *HTC* of 30 and 40 $W \cdot m^{-2} \cdot K^{-1}$ are included to show how the latter captures the physical results more closely. Experimental data are represented with square markers. Overall, simulation results with an *HTC* of 40 $W \cdot m^{-2} \cdot K^{-1}$ agreed better with the experimental data.

Discrepancy from the Tracey and McCown (1934) study was roughly 9% for 30 $W \cdot m^{-2} \cdot K^{-1}$ and 2% for 40 $W \cdot m^{-2} \cdot K^{-1}$. The agreement is quite satisfactory when considering the various sources of uncertainty. The experimental data contained instrumentation and potential human error. The composition of the homogeneous material and the comparison ice cream were likely different. The boundary conditions were idealized, and there was also the inherent nature of approximation for the simulation.

3.2 Model 3.2: Single Phase Cubical and Model 3.3: Multiphase Cubical

Model 3.1 provided a convenient method for validating the ice cream heat transfer approach. The validated model was then used to bridge to the ice phase change results of Russell et al. (1999). For parametric study, the simulation was repeated varying only the geometry and draw temperature from Model 3.1. The single phase cubical study (Model 3.2) took 64 min to achieve a warmest point temperature of -18°C (θ = 0.56). Note that the dimensionless temperature of Models 3.2 and 3.3 had a different normalization basis than that of Model 3.1 since the cube ambient temperature was -35°C. For Model 3.1, the ambient temperature was -30°C. The multiphase model (Model 3.3) had nearly the same response as the single phase (Model 3.2). Figure 3.4 shows a comparison of the temperature histories of the two models along with the two experimental data points provided in the comparison study (Russell et al., 1999). The experimental specimen hardened (attained warmest temperature of -18°C) in about an hour.

Models 3.2 and 3.3 each hardened in 64 min for an *HTC* of 30 $W \cdot m^{-2} \cdot K^{-1}$. This duration is close to the approximate time of 60 min reported by Russell et al. (1999). Figure 3.5 shows the temperature contours of Model 3.2 at 64 min, which resemble the results of Model 3.1 closely. They are also nearly identical to the temperature contours of Model 3.3 at the same hardening time, shown in Figure 3.6.

With the accurate temperature characteristics of Model 3.2, Model 3.3 was equipped to simulate the ice crystal morphology of the hardening process. The phase change results mirror the temperature distribution displayed by Model 3.2. Figure 3.7 extends the results of Figure 3.6 to show the corresponding ice distribution at 64 min. The maximum occurs along the edges and exterior corners of the cube, while the minimum occurs in the ice cream center. The evolution of the ice volume fraction is compared with the previously published experimental results in Figure 3.8. The numerical results silhouette the overall empirical behavior, but ultimately fall slightly below the final mean crystal length of the experimental results. This is probably due to the fact that aggregation and other crystallization kinetics have not been modeled in this study. When greater numerical data is available for recrystallization, the current model can be improved.

The population balance results also provide detailed information on the ice crystal size of the frozen product. Figure 3.9 shows the CSD at the completion of the hardening process (64 min). The average crystal length is approximately 35 μm, which falls short of the experimentally-obtained 40 to 55 μm range reported by Russell et al. (1999). These CSD results show that the population balance model is becoming a viable design tool for the ice cream manufacturer.

4. Conclusions

The hardening process is an important and intriguing step in ice cream manufacturing. Accurately modeling its heat transfer and ice phase changes is inherently challenging. The process has been simulated here through the following three-part model progression: (1) a single-phase cylinder with temperature-dependent material properties was validated with previous experimental data, (2) the single-phase material was then reconfigured into a cube, and (3) the cubical model was advanced to a multiphase PBM approach. The single phase results showed that the homogeneous ice cream material was very accurate in capturing the heat transfer characteristics of the actual ice cream mix. The crystalline microstructure was then constructed through a combination of commercial heat transfer and population balance software with user subroutines for crystal nucleation and growth kinetics. The final crystallization results were verified with previous experimental research. The predicted average crystal length of 35 μm is smaller than the 40-55 μm range reported in the literature (Russell et al., 1999), though the value is reasonably close. The work shows that population balance equations are becoming increasingly useful ice cream manufacturing. The current approach is flexible and efficient for predicting the CSD throughout the ice cream hardening process. The computational method is applicable for myriad food-freezing processes, alloy solidification, and other multiphase systems.

References for Chapter 3

Adapa S, Schmidt KA, Jeon IJ, Herald TJ, Flores RA. 2000. Mechanisms of Ice Crystallization and Recrystallization in Ice Cream: a Review. Food Rev Int 16:259-71.

Aldazabal J, Martin-Meizoso A, Martinez-Esnaola JM, Farr R. 2006. Deterministic Model for Ice Cream Solidification. Comp Mat Sci 38:9-21.

Ben-Yoseph E, Hartel RW. 1998. Computer Simulation of Ice Recrystallization in Ice Cream During Storage. J Food Eng 38:309-29.

Cindio BD, Iorio G, and Romano V. 1985. Thermal Analysis of the Freezing of Ice Cream Brickettes by the Finite Element Method. J Food Sci 50:1463-6.

Cogne C, Andrieu J, Laurent P, Besson A, Nocquet J. 2003. Experimental Data and Modelling of Thermal Properties of Ice Creams. J Food Eng 58:331-41.

Cook KLK, Hartel RW. 2010. Mechanisms of Ice Crystallization in Ice Cream Production. Compr Rev Food Sci Food Safety 9:213-22.

Cordell JM, Webb DC. 1985. The freezing of ice cream. Proceedings of the Int Symp Heat and Mass Transfer Prob in Food Eng [Accessed in: Thermal analysis of the freezing of ice cream brickettes by the Finite Element Method; de Cindio et al. (1985)]; 1972 October 24-27; Wageningen, NL. J Food Sci 50:1464.

Crilly JF, Russell AB, Cox AR, Cebula DJ. 2008. Designing Multiscale Structures for Desired Properties of Ice Cream. Ind Eng Chem Res 47:6362-7.

Cromer WC, Miller MJ, Xin XJ, Pei ZJ, Schmidt KA. Effects of Container Geometry on Energy Consumption During Hardening in Ice Cream Manufacturing. Proc MSEC 2010, Ed. ASME, Erie, Pennsylvania, USA, 2010 Oct 12-15th.

Fellows PJ. 2000. Food Processing Technology Principles and Practices. 2nd ed. New York: CRC Press.

Fluent Inc. 2006. Fluent 6.3. Lebannon, NH.

Hounslow MJ, Ryall RL, Marshall VR. 1988. A Discretized Population Balance for Nucleation, Growth, and Aggregation. AIChE J 34:1821-32.

Hulburt HM, Katz S. 1964. Some Problems in Particle Technology - a Statistical Mechanical Formulation. Chem Eng Sci 19:555-74.

Incropera FP, DeWitt DP, Bergman TL, Lavine AS. 2007. Fundamentals of Heat and Mass Transfer. 6th ed. Hoboken, NJ: John Wiley.

Lian G, Moore S, Heeney L. 2006. Population Balance and Computational Fluid Dynamics Modelling of Ice Crystallization in a Scraped Surface Freezer. Chem Eng Sci 61:7819-26.

Litster JD, Smit DJ, Hounslow MJ. 1995. Adjustable Discretized Population Balance for Growth and Aggregation. AIChE J 41:591-603.

Marshall RT, Goff HD, Hartel RW. 2003. Ice Cream. 6th ed. New York: Kluwer Academic/Plenum Publishers.

Ramkrishna D. 2000. Population Balances: Theory and Applications to Particulate Systems in Engineering. San Diego, CA: Academic Press.

Randolph AD, Larson MA. 1988. Theory of Particulate Processes. 2nd ed. New York: Academic Press.

Rauth NL, Miller MJ, Xin XJ, Pei ZJ, Schmidt KA. Effects of Air Flow, Draw Temperature and Boundary Conditions on Hardening in Ice Cream Manufacturing. Proc MSEC 2010, Ed. ASME, Erie, Pennsylvania, USA, 2010 Oct 12-15th.

Regand A, Goff HD. 2005. Freezing and Ice Recrystallization Properties of Sucrose Solutions Containing Ice Structuring Proteins from Cold-Acclimated Winter Wheat Grass Extract. J Food Sci 70:E552-6.

Russell AB, Cheney PE, Wantling SD. 1999. Influence of Freezing Conditions on Ice Crystallisation in Ice Cream. J Food Eng 39:179-191.

Tracey PH, McCown CY. 1934. A study of factors related to the hardening of ice cream. J Dairy Sci 17:47-60.

Wildmoser H, Scheiwiller J, Windhab EJ. 2004. Impact of Disperse Microstructure on Rheology and Quality Aspects of Ice Cream. Lebensm-Wiss Technol 37:881-91.

Woo XY, Tan RBH, Chow PS, Braatz RD. 2006. Simulation of Mixing Effects in Antisolvent Crystallization Using a Coupled CFD-PDF-PBE Approach. Cryst Growth Des 6:1291-303.

Zheng L, Sun DW. 2006. Innovative Applications of Power Ultrasound During Food Freezing Processes - a Review. Trends Food Sci Tech 17:16-23.

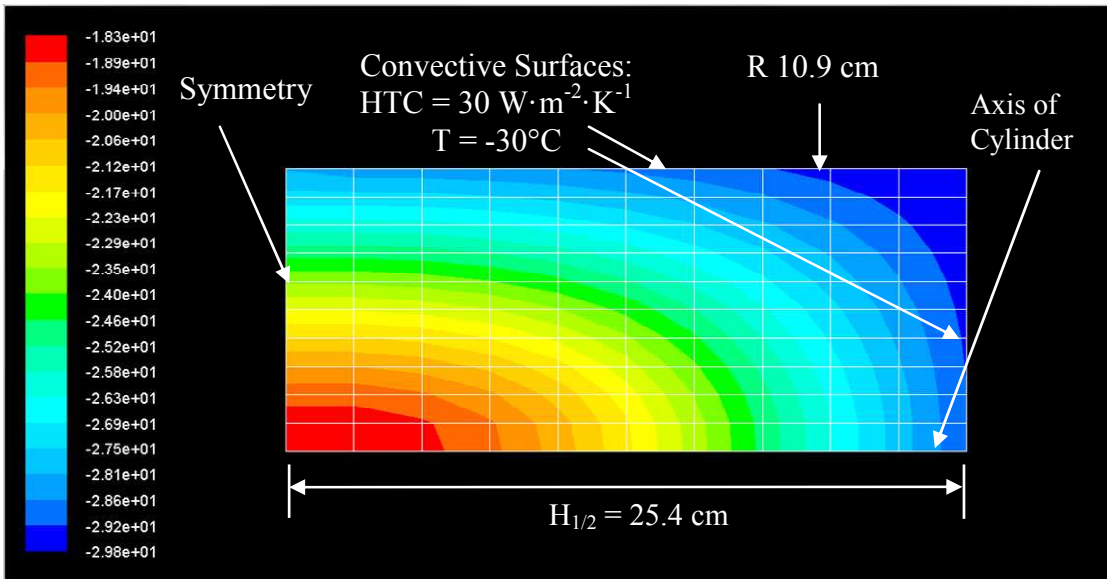

Figure 3.1 Dimensions and boundary conditions for Model 3.1.

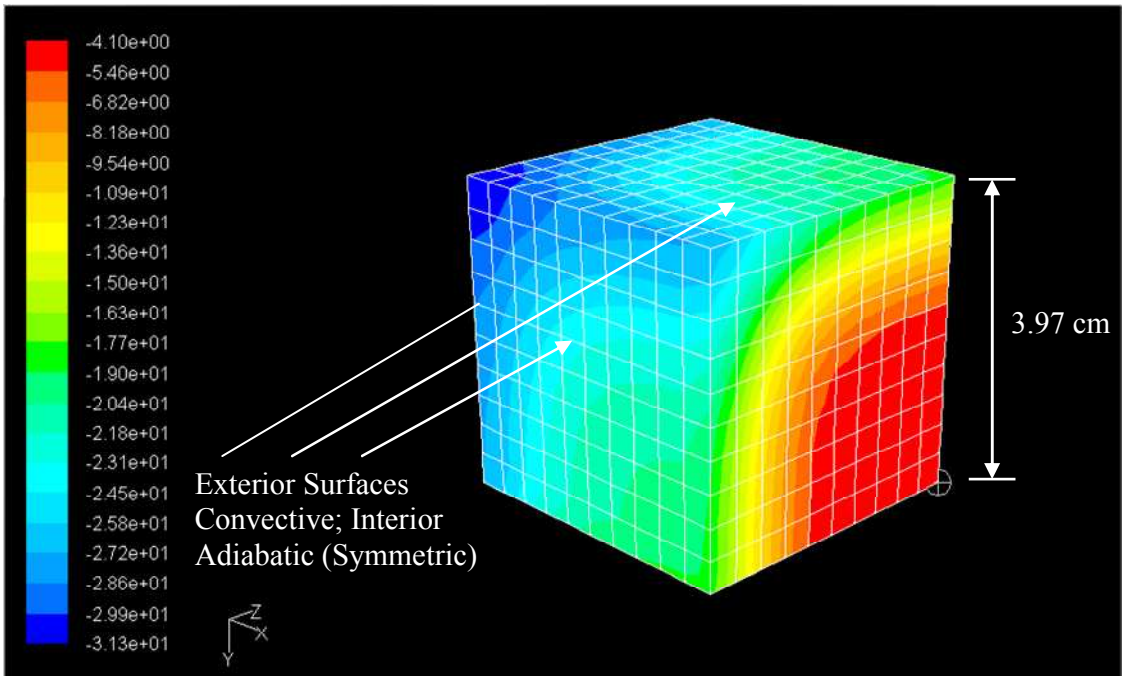

Figure 3.2 Cubical setup with Model 3.2 temperature contours at 20 min.

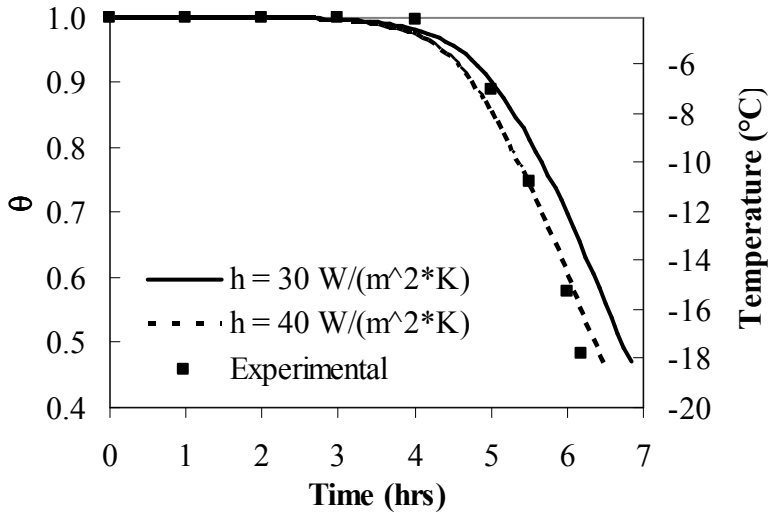

Figure 3.3 Temperature history plot for center point of Model 3.1.

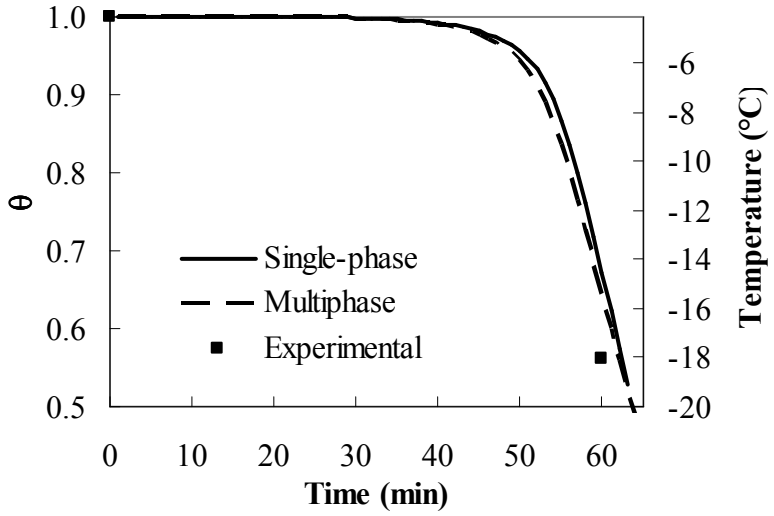

Figure 3.4 Temperature history comparison for Models 3.2 and 3.3.

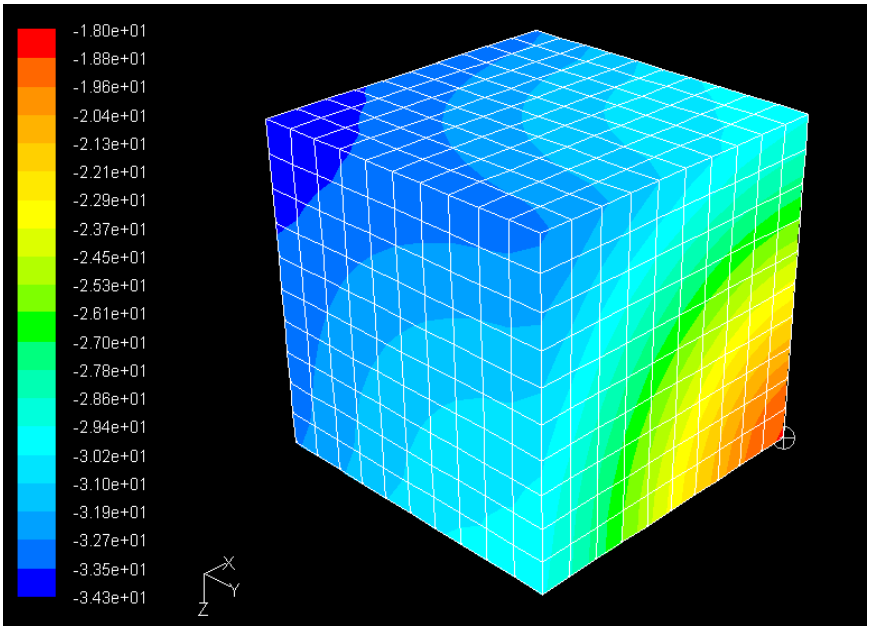

Figure 3.5 Model 3.2 temperature contours at hardening completion (64 min).

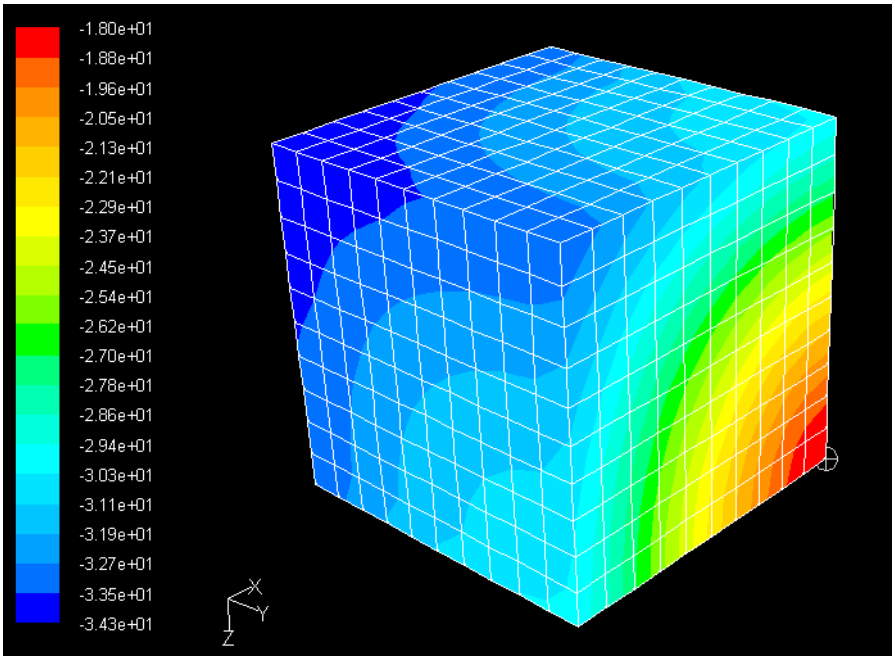

Figure 3.6 Model 3.3 temperature contours at 64 min.

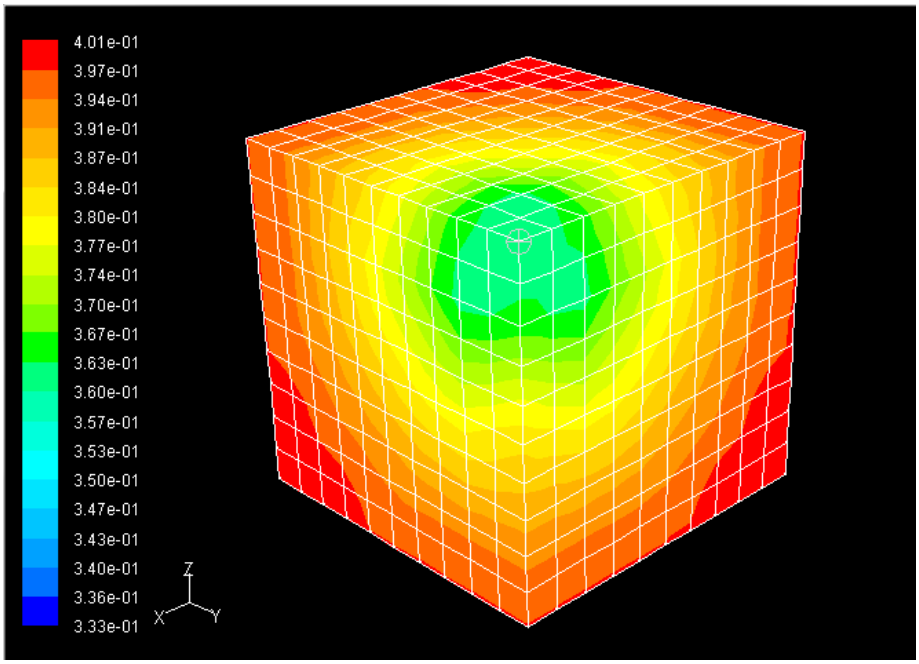

Figure 3.7 Model 3.3 ice volume fraction at 64 min.

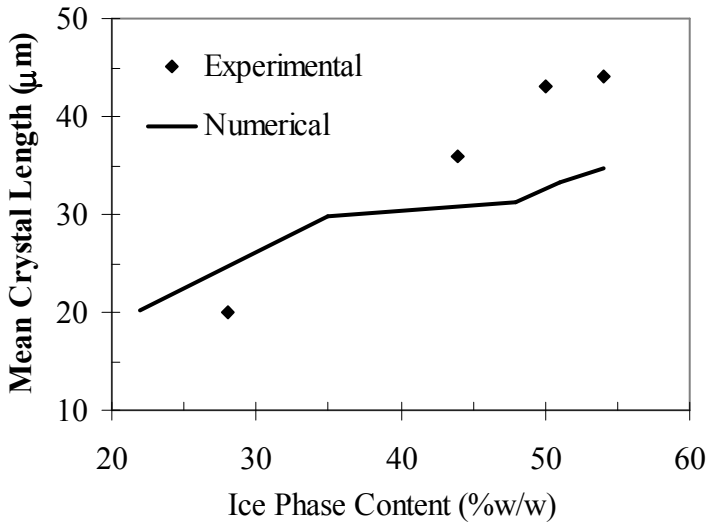

Figure 3.8 Comparison of Russell et al. (1999) and PBM calculated mean crystal length versus ice phase content.

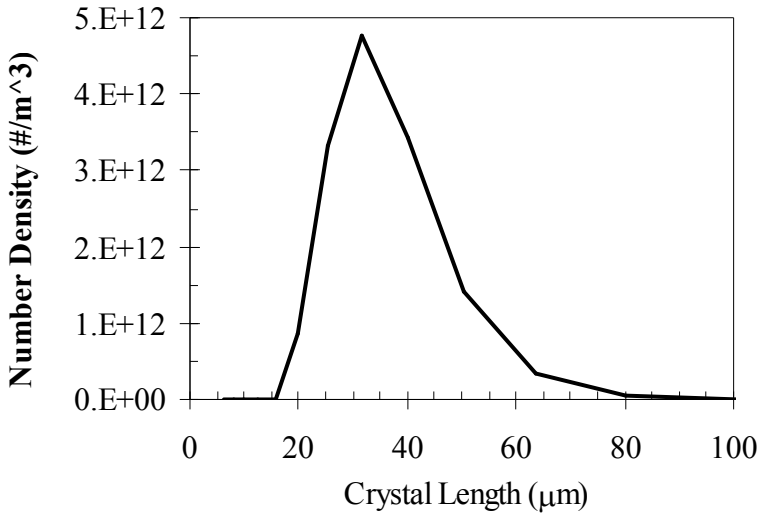

Figure 3.9 Volume-averaged crystal size distribution (CSD) after 64 min of residence time.

Chapter 4 - Combined Computational Fluid Dynamics and Population Balance Freezing

Abstract

Freezing is the single most influential step of ice cream manufacturing. During freezing, multiphase flow, ice crystal nucleation and growth, phase change, and viscous shearing all play roles in ice cream crystallization. In this work, ice crystallization of a sucrose solution is investigated using a coupled computational fluid dynamics and population balance method. The dynamic freezing process that takes place in a scraped surface heat exchanger (SSHE) is simulated using a sucrose solution as a model material. Ice crystal nucleation and growth kinetics are described by population balance equations. Effects of multiphase, phase change, and shearing from scraping in a continuous freezer on ice cream formation are investigated, and the fluid flow, temperature distribution and ice crystal size are predicted. The method predicts trends similar to experimental observations, and provides insight into how processing conditions affect ice cream manufacturing.

1. Introduction

The objective of this work is to simulate the dynamic freezing process that takes place in a scraped surface heat exchanger (SSHE) and gain insight of the freezing process. Energy consumption by the dairy food industry in the United States constitutes 10% of all energy consumed by the U.S. food industry. The knowledge from this research will be helpful in the investigation of energy consumption in cooling and refrigeration of foods.

A sucrose solution was used as a simplified model to simulate the more complex ice cream mix, and the crystallization dynamics are described using population balance equations (PBE). The challenge with the freezing processes is to undergo crystallization quickly enough to produce an acceptable final product. For ice cream, the critical size at which coarseness becomes apparent is around 55 μm, but the value also depends on crystal shape and distribution (Marshall et al., 2003). Most studies on SSHE ice crystallization have focused on the mechanisms of crystallization through experimentation as reviewed by Adapa et al. (2000), and demonstrated by Flores and Goff (1999); Russell et al. (1999).

Examples of crystallization simulations include those by Hey and MacFarlane (1998); Shirai et al. (1986). Those models were based on the population balance equations (PBE) introduced by Hulburt and Katz (1964), and applied to crystallization by Randolph and Larson (1988). Randolph and Larson tailored PBE to crystallization using mixed suspension mixed product removal (MSMPR). PBE have also been applied to lactose crystallization by Griffiths et al. (1982); Shi et al. (1990). *Engineering Aspects of Milk and Dairy Products* provides a wealth of information on dairy crystallization topics (dos Reis Coimbra and Teixeira, 2010). Recent studies have integrated PBE within computational fluid dynamics (CFD). This was done by Woo et al. (2006); Lian et al. (2006). Those studies assumed transient two- and one-dimensional geometries, respectively.

The contribution of the present work is to apply the coupled CFD-PBE method to a process scale SSHE using a commercially available PBE package (Fluent 6.3, 2006). Previous SSHE crystallization studies required user subroutines for mass transfer between phases (Woo et al., 2006; Lian et al., 2006). This work utilizes the Population Balance Model (PBM) available for Fluent 6.3, and it also investigates the effects of varying initial sucrose concentration.

The paper is organized as follows. The model is described in Section 2, and results are discussed in Section 3. Conclusions are then presented in Section 4, and future work is discussed in Section 5.

2. Materials and Methods

The geometry for this analysis was obtained from the SSHE currently being used at the Dairy Processing Plant of Kansas State University (KSU), located in Call Hall on campus. The continuous freezer has a throughput of approximately 390 L/hr (100 gal/hr). It rotates at roughly 250 rpm, and its freezing temperature at the barrel wall is estimated to be -15°C. The dasher and other internal components of the Cherry-Burrell Freezer are shown in Figure 4.1. The 3D domain of simulation and the center-most section, which was actually modeled for the analysis, are indicated in Figure 4.1.

Several assumptions were made to simplify the simulation, including the following:

1. Throughput flow and freezing are steady.
2. Sucrose solution viscosity is constant. This allows for modeling a 2D cross section of the freezer.
3. Backmixing is negligible.
4. Heat due to blade-barrel contact is negligible.
5. Crystals are spherical; crystal size refers to diameter.
6. Only crystal nucleation and growth kinetics are modeled.
7. Energy and PBE calculations are implicitly coupled; this is explained in greater detail in the subsequent paragraphs.

The simplified 2D geometry is shown in Figure 4.2 along with the unstructured mesh. About 17000 cells were used to model the geometry. For reference the barrel diameter is 0.1016 m (4 in). The flow problem was solved using a rotating reference frame; the direction of rotation is indicated in Figure 4.2. Most of the zones were stationary relative to the rotating frame; the zones and their corresponding boundary conditions are given in Table 4.1.

Fluid flow was modeled using the Eulerian multiphase model, which allows for multiple separate yet interacting phases (Fluent 6.3, 2006). The primary phase was sucrose solution, while the secondary phase was ice. Material properties were obtained from previous literature (Woo et al., 2006; Lian et al., 2006). The sucrose solution properties were: density of 1100 $kg \cdot m^{-3}$, specific heat capacity of 3564 $J \cdot kg^{-1} \cdot K^{-1}$, thermal conductivity of 0.489 $W \cdot m^{-1} \cdot K^{-1}$, and viscosity of 0.01 $kg \cdot m^{-1} \cdot s^{-1}$.

As with other CFD software, Fluent solves Conservation of Mass and Momentum (Fluent 6.3, 2006). Their multiphase representations are shown in Equations 4.1 and 4.2. The subscripts q and p refer to the q^{th} and p^{th} phases, respectively. Mass transfer from p to q is denoted by $\dot{m}_{pq}$. Initially all mass was contained in the sucrose phase (p). When conditions were appropriate for crystallization ($T<T_f$ and $\theta<\theta_e$, as explained in the following section), ice mass was nucleated and proceeded to grow. This mass was transferred directly from phase p to q; that is $\dot{m}_{pq}$ was used to model the freezing process. Freezing point depression was simulated implicitly through the use of power laws, which are detailed in Equations 4.3-4.6. Using this method precluded the need to model species transport. The last term of Equation 4.1, S_q, is a mass source term; in this simulation it is zero. $\bar{\bar{\tau}}_q$ is the q^{th} strain tensor. It is defined for each individual phase.

$$\frac{\partial}{\partial t}\left(\alpha_q \rho_q\right)+\nabla\cdot\left(\alpha_q \rho_q \vec{v}_q\right)=\sum_{p=1}^{n}\left(\dot{m}_{pq}-\dot{m}_{qp}\right)+S_q \tag{4.1}$$

$$\frac{\partial}{\partial t}\left(\alpha_q \rho_q \vec{v}_q\right)+\nabla\cdot\left(\alpha_q \rho_q \vec{v}_q \vec{v}_q\right)=-\alpha_q \nabla p\cdot\bar{\bar{\tau}}_q+\alpha_q \rho_q \vec{g}+\sum_{p=1}^{n}\left(\vec{R}_{pq}+\dot{m}_{pq}\vec{v}_{pq}-\dot{m}_{qp}\vec{v}_{qp}\right)+\vec{F}_q+\vec{F}_{lift,q}+\vec{F}_{vm,q} \tag{4.2}$$

PBE proceeded using power laws of ice volume fraction within user subroutines. The method is similar to that presented by Lian et al. (2006) which employed ice mass fraction. Equation 4.3 was used to calculate freezing temperature (T_f), and Equation 4.4 was used to calculate equilibrium ice content (θ_e) for temperatures below T_f. The equilibrium ice content was calculated using initial sucrose concentrations (c_0) of 0.25 and 0.15 by weight, which correspond to freezing temperatures of -2.1 and -1.1°C respectively. These values were paired with the equilibrium ice content, and were fitted to empirical crystallization data (Lian et al., 2006). That information was used to determine growth constants k_b and k_g, as well as power indices n_b and n_g. K_b was set at 4.0e13 #·m^{-3}·s^{-1}, and n_b was 1. A value of 6.0e-6 m·s^{-1} was used for k_g, and n_g was 2. Equations 4.5 and 4.6 show how the nucleation ($\dot{n}_0$) and growth (G_L) terms were calculated. Note that G_L refers to crystal growth based on length. θ_i is the ice fraction at a specific time step based on the given cell temperature (T).

$$T_f=\frac{5c_0}{c_0-0.85} \tag{4.3}$$

$$\theta_e=1-c_0\left(\frac{T-5}{0.85T}\right) \tag{4.4}$$

$$\dot{n}_0=k_b\left(1-\frac{\theta_i}{\theta_e}\right)^{n_b} \tag{4.5}$$

$$G_L = k_g \left(1 - \frac{\theta_i}{\theta_e}\right)^{n_g} \tag{4.6}$$

Three population balance techniques are available using the PBM of Fluent 6.3: Discrete, Standard Moment, and Quadrature Moment. Crystallization in this simulation was carried out using the Discrete Method of PBE developed by Hounslow et al. (1988), Litster et al. (1995), and Ramkrishna (2000). Fourteen discrete bin sizes were created using a geometric ratio definition from the PBM interface. Crystal size distribution ranged from Fluent PBE can be expressed by Equation 4.7. Here *n(V,t)* refers to crystal density (#·m^{-3}) as a function of crystal volume (V) and time (t).

$$\frac{\partial}{\partial t}\left[n(V,t)\right] + \nabla \cdot \left[\vec{u}n(V,t)\right] + \nabla_V \cdot \left[G_V n(V,t)\right] = B_{ag} + B_{br} - D_{ag} - D_{br} \tag{4.7}$$

In this model the right-hand side of 4.7 is zero, since only nucleation and growth are taken into account; aggregation and breakage terms are excluded. Equation 4.7 is subject to the boundary and initial conditions of Equations 4.8 and 4.9.

$$n(V, t=0) = n_V \tag{4.8}$$

$$G_V n(V=0, t) = \dot{n}_0 \tag{4.9}$$

Two separate cases were modeled here: (1) an initial sucrose concentration of 0.25 was simulated for comparison with the results of Lian et al. (2006) and (2) an initial sucrose concentration of 0.15 was modeled to investigate the effect of varying sucrose content. Both of

the simulations were performed in three stages. First the steady state background flow field was calculated, and then the transient calculations were performed. The software yielded more meaningful results by separating the transient heat transfer and crystallization studies, so the energy field was calculated prior to the crystal distribution. Fluent solves the Energy Equation in the form given by Equation 4.10 (Fluent 6.3, 2006):

$$\frac{\partial}{\partial t}(\rho E) + \nabla \cdot [\vec{v}(\rho E + p)] = \nabla \cdot \left[k_{eff} \nabla T - \sum h_j J_j + \left(\bar{\bar{\tau}}_{eff} \cdot \vec{v} \right) \right] + S_h \tag{4.10}$$

Here the first three terms of the right-hand side of Equation 4.10 represent energy transfer associated with conduction, species diffusion, and viscous dissipation. S_h refers to the heat of chemical reaction and any other volumetric heat sources modeled (zero in this simulation). Transient calculations were performed for 20 sec of energy transfer followed by 20 sec of crystallization. This effectively simulated a total calculation time of 20 sec, which roughly corresponds to the time required to freeze 1.89 L of ice cream using the KSU continuous freezer. Material properties are different between the two fluids, but the comparison provides a baseline for simulation.

3. Results and Discussion

The first output from the simulation was the initial sucrose solution flow field. Flow results in the form of relative velocity vectors are shown in Figure 4.3. The greatest disturbance can be seen in the wake of the rotator or beater (zone 4 of Figure 4.2). Small vortices are developed in these four regions as well as in the wakes of the dasher tube sections. Another

distinct feature of the flow field is the swirling effect around the center bar, which is a result of the relative translational velocity imposed there. The translational velocity was modeled to capture disturbance caused by the difference in rotation between the center bar and fluid. The background flow field impacts all of the subsequent calculations.

The next stage of simulation was achieved by deactivating the flow equations and activating the energy equations. Fluent has a convenient control interface for this purpose. The simulation type was also changed from steady to unsteady. Transient calculations were performed for 20 sec using the boundary conditions outlined in Table 4.1. The coldest region developed directly along the barrel wall, as shown in Figure 4.4. The warmest portion was contained between the rotator and center bar zones. The temperature there was above the freezing temperature calculated by Equation 4.3, so the corresponding ice content was zero there.

Once the energy field was calculated, the energy equation was deactivated, and volume fraction and phase-2 bin equations were activated. Volume fraction handles phase change, and phase-2 bin models PBE nucleation and growth. The simulation ran for an 'additional' 20 sec; in actuality the previous 20 sec were simulated again to incorporate mass transfer between the phases. Ice volume fraction is shown in Figures 4.5 and 4.6 for the different initial sucrose concentrations.

These figures reveal that the PBM calculated the greatest ice fraction along the barrel walls; the same locations as the coldest temperatures of sucrose solution. The results show the scraping action of the blades. The ice fraction reaches a maximum of 1.0 before it is deflected back into the cooled mix. The volume fraction contours also reflect the background flow field by indicating the small vortices in the wakes of the dasher tube sections. Portions of ice can even be seen being agitated by the rotator sections. The figures show more ice was formed for the 15%

initial sucrose solution, which is attributed to its warmer freezing temperature. Other general characteristics are similar to the previous computations.

The real usefulness of PBE is the ability to predict crystal size distribution (CSD). Charts of number density versus crystal diameter are shown in Figures 4.7 and 4.8. For the given phase properties and operating conditions, the average crystal size was roughly 9 μm. The CSD is comparable to previously reported sucrose crystallization data (Lian et al., 2006). The figures indicate that more crystals are present in the 0.15 initial sucrose solution mix, but the overall CSD is similar.

4. Conclusions

PBE have been shown to be flexible and accurate through previous research (Woo et al., 2006; Lian et al., 2006). The add-on module (PBM) offered by Fluent captures the versatility of the method in a reasonably straightforward package. Operating conditions can be varied conveniently to produce physically satisfactory results. The model presented in this study shows that the PBM can be used to predict ice crystal fraction and distribution. Having this information enables parametric study of the freezing process for the purpose of quality control and energy reduction. This study also serves as a benchmark for varying phase properties, which will in turn provide a bridge for modeling the complex material properties of ice cream mix. Energy efficiency in ice cream production is an important topic given the prolific usage requirements of the dairy industry.

References for Chapter 4

Adapa S, Schmidt KA, Jeon IJ, Herald TJ, Flores RA. 2000. Mechanisms of Ice Crystallization and Recrystallization in Ice Cream: a Review. Food Rev Int 16:259-71.

Flores AA, Goff HD. Ice Crystal Size Distributions in Dynamically Frozen Model Solutions and Ice Cream as Affected by Stabilizers. J Dairy Sci 82:1399-407.

Fluent Inc. 2006. Fluent 6.3. Lebannon, NH.

Griffiths RC, Paramo G, Merson RL. Preliminary Investigation of Lactose Crystallization Using the Population Balance Technique. AIChE Symposium Series 218:118-28.

Hey JM, MacFarlane DR. 1998. Crystallization of Ice in Aqueous Solutions of Glycerol and Dimethyl Sulfoxide 2: Ice Crystal Growth Kinetics. Cryobiology 37:119-30.

Hounslow MJ, Ryall RL, Marshall VR. 1988. A Discretized Population Balance for Nucleation, Growth, and Aggregation. AIChE J 34:1821-32.

Hulburt HM, Katz S. 1964. Some Problems in Particle Technology - a Statistical Mechanical Formulation. Chem Eng Sci 19:555-74.

Lian G, Moore S, Heeney L. 2006. Population Balance and Computational Fluid Dynamics Modelling of Ice Crystallization in a Scraped Surface Freezer. Chem Eng Sci 61:7819-26.

Litster JD, Smit DJ, Hounslow MJ. 1995. Adjustable Discretized Population Balance for Growth and Aggregation. AIChE J 41:591-603.

Marshall RT, Goff HD, Hartel RW. 2003. Ice Cream. 6th ed. New York: Kluwer Academic/Plenum Publishers.

Mathlouthi M, Reiser P. 1995. Sucrose Properties and Applications. London, UK: Blackie Academic & Professional.

Ramkrishna D. 2000. Population Balances: Theory and Applications to Particulate Systems in Engineering. San Diego, CA: Academic Press.

Randolph AD, Larson MA. 1988. Theory of Particulate Processes. 2nd ed. New York: Academic Press.

Reis Coimbra DJS, Teixeira JA. 2010. Engineering Aspects of Milk and Dairy Products. Boca Raton, FL: CRC Press Taylor and Francis Group, LLC.

Russell AB, Cheney PE, Wantling SD. 1999. Influence of Freezing Conditions on Ice Crystallisation in Ice Cream. J Food Eng 39:179-91.

Shi Y, Liang B, Hartel RW. Crystallization Kinetics of Alpha-Lactose Monohydrate in a Continuous Cooling Crystallizer. J Food Sci 55:817-20.

Shirai Y, Sakai K, Nakanishi K, Matsuno R. 1986. Analysis of Ice Crystallization in Continuous Crystallizers Based on a Particle Size-dependent Growth Rate Model. Chem Eng Sci 41:2241-6.

Woo XY, Tan RBH, Chow PS, Braatz RD. 2006. Simulation of Mixing Effects in Antisolvent Crystallization Using a Coupled CFD-PDF-PBE Approach. Cryst Growth Des 6:1291-303.

Nomenclature for Chapter 4

Letters

B	Crystal birth
c_0	Initial concentration
D	Crystal death
E	Energy
$\vec{F}_{lift,q}$	Lift force
$\vec{F}_q$	External body force
$\vec{F}_{vm,q}$	Virtual mass force
$\vec{g}$	Gravitational acceleration
G_L	Growth Rate based on length, $m \cdot s^{-1}$
G_V	Growth Rate based on volume, $m^3 \cdot s^{-1}$
h_j	Sensible enthalpy of species j
J_j	Diffusion flux
k_b	Nucleation constant, $\# \cdot m^{-3} \cdot s^{-1}$
k_{eff}	Effective thermal conductivity, $W \cdot m^{-1} \cdot K^{-1}$
k_g	Growth constant, $m \cdot s^{-1}$
$\dot{m}_{pq}$	Mass transfer from phase p to q.
n	Population density, $\# \cdot m^{-3}$
$\dot{n}_0$	Initial nucleation rate, $\# \cdot m^{-3} \cdot s^{-1}$
n_b	Nucleation index
n_g	Growth index
n_V	Initial population density, $\# \cdot m^{-3}$
p	Pressure shared by all phases
$\vec{R}_{pq}$	Interaction force between phases
S_q	Mass source, $kg \cdot s^{-1}$
S_h	Volumetric heat source, $W \cdot m^{-3}$
t	Time, sec
T_f	Freezing Temperature, °C
$\vec{u}$	Crystal velocity, $m \cdot s^{-1}$
V	Volume, m^3
$\vec{v}_{pq}$	Phase velocity, $m \cdot s^{-1}$

Symbols

α	Mass and thermal diffusivities
ρ	Density, $kg \cdot m^{-3}$
$\bar{\bar{\tau}}_{eff}$	Stress-strain tensor of phase q
θ_i	Volume fraction of ice
θ_e	Equilibrium ice content

Subscripts

ag	Aggregation
br	Breakage
p	Subscript for phase p
q	Subscript for phase q

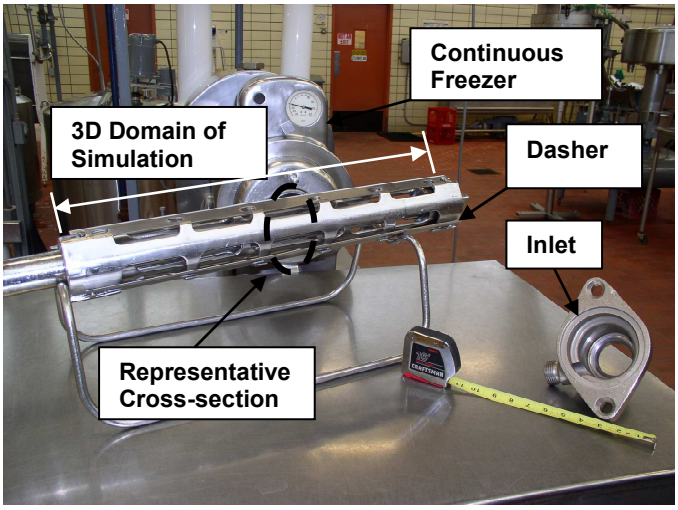

Figure 4.1 Components of the KSU Freezer

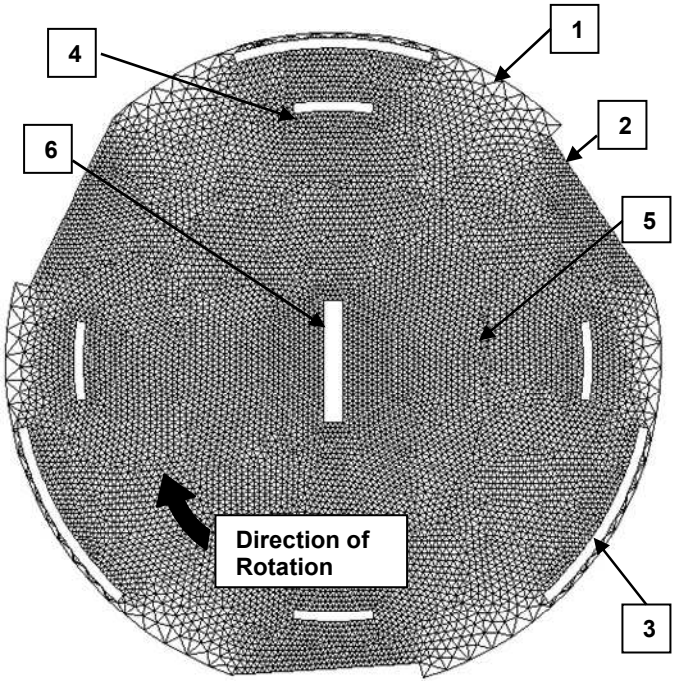

Figure 4.2 CFD-PBE Model Conditions

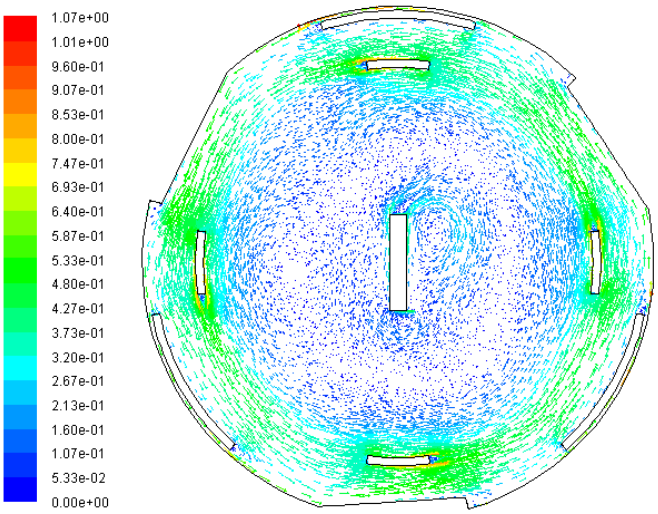

Figure 4.3 Relative Velocity Vectors Colored by Relative Velocity Magnitude in m/s

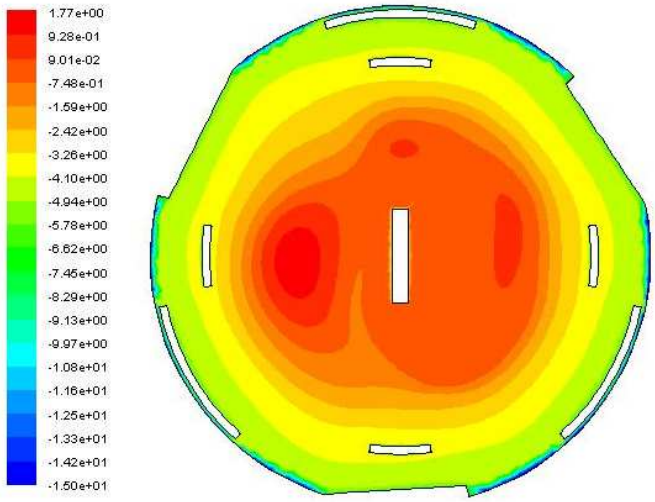

Figure 4.4 Temperature Distribution (in °C) after 20 sec of Dwell Time in the Freezer

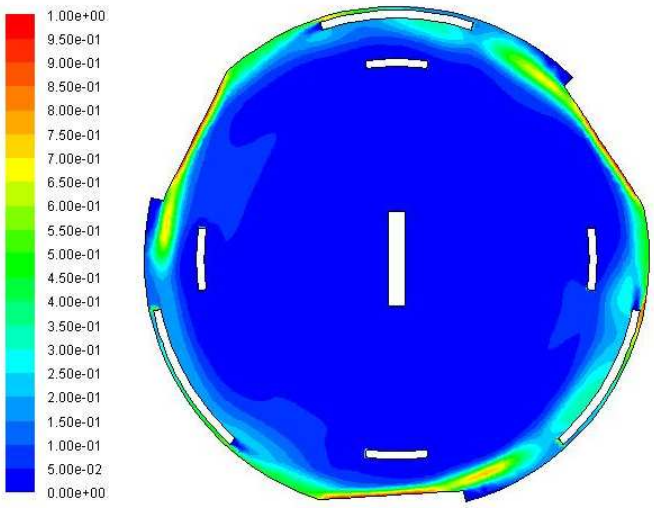

Figure 4.5 Ice Fraction for 0.25 Sucrose Soln. after 20 sec of Dwell Time in the Freezer

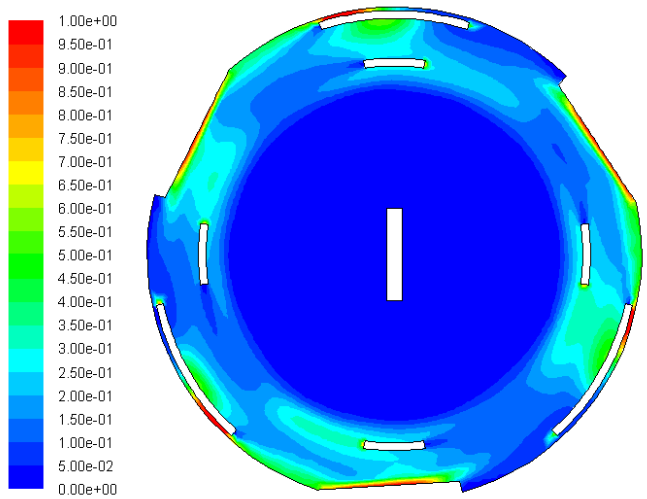

Figure 4.6 Ice Fraction for 0.15 Sucrose Soln. after 20 sec of Dwell Time in the Freezer

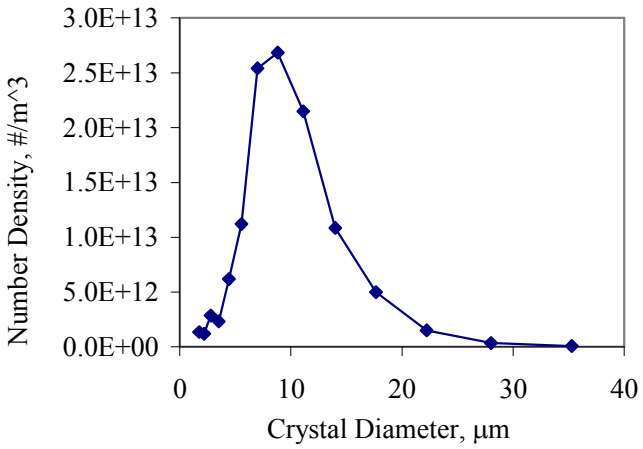

Figure 4.7 Discrete Crystal Number Density Based on Volume-Average for 0.25 Sucrose Soln. after 20 sec of Dwell Time

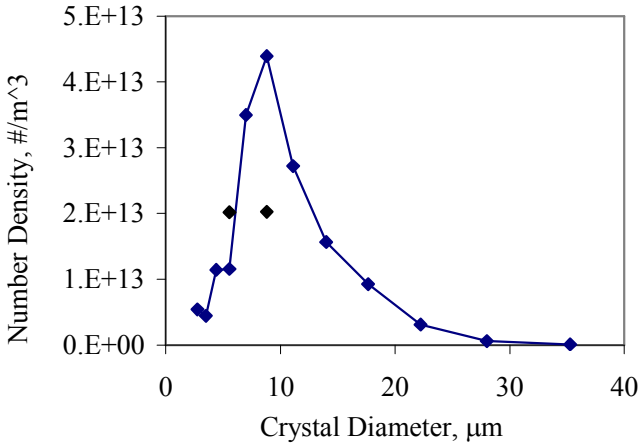

Figure 4.8 Discrete Crystal Number Density Based on Volume-Average for 0.15 Sucrose Soln. after 20 sec of Dwell Time

Table 4.1 Zones and Boundary Conditions

Number	Description	Momentum BC	Thermal BC (°C)
1	Barrel	Stationary, Absolute Frame	Constant: -15
2	Blade	Stationary, Relative to Fluid	Constant: -5
3	Dasher Tube	Stationary, Relative to Fluid	Constant: -5
4	Rotator (Beater)	Stationary, Absolute Frame	Constant: -5
5	Fluid	Rotating 250 rpm (counterclockwise)	Initial: 5
6	Center Bar	0.5 m/s (**i** + **j**) Relative to Fluid	Constant: -3

Chapter 5 - Conclusions and Future Work

1. Thesis Discussion

Ice cream manufacturing has been described and modeled in this work. Reducing total energy consumption in the process is a key industrial issue. Several models have been presented to simulate the freezing and hardening steps. As with any computational studies, these simulations have been built on simplifying assumptions. Higher levels of physical accuracy can be obtained through more rigorous treatment of the multiphase phenomenon in ice cream manufacturing.

For a more precise continuous freezing model, a non-Newtonian ice cream material must be included in the simulation. Currently, a constant viscosity sucrose solution has been utilized. Furthermore, for complete end-to-end energy savings, the freezing and hardening studies must be interconnected. It would also be beneficial to include the storage process. Nevertheless, the current work provides a valuable baseline for future research.

The models presented here yield several important insights for ice cream simulation. Specifically, single and multiphase approaches have been reported. Energy saving configurations have been outlined and quantified for the ice cream hardening process. Moreover, complex ice crystal morphology has been modeled through the use of discrete population balance equations. Given the applications and fundamental knowledge discussed in this work, energy savings in ice cream manufacturing has been shown to be both relevant and intriguing.

2. Thesis Conclusions

2.1. FEA Hardening

Ice cream manufacturing is comprised of several important processes to create a product with desirable qualities. The hardening process has a significant impact on the quality of the final product. In Chapter 2, finite element models were used to investigate the hardening process. Temperature dependent properties were retrieved from previous empirical studies. Simulation results were compared with previously published experimental data (Tracy and McCown 1934). The results were shown to be accurate within 2% for a heat transfer coefficient (HTC) of 40 $W \cdot m^{-2} \cdot K^{-1}$.

The study elucidates optimal conditions for energy efficiency in the ice cream hardening step. The coefficient for convection-conduction control transition, h_{CCCT}, is characterized by a Biot number in the range of 1.5 to 5. For a gallon of typical ice cream, h_{CCCT} is 23 to 77 $W \cdot m^{-2} \cdot K^{-1}$. Increasing the convective coefficient up to h_{CCCT} by increasing air flow or decreasing air temperature shortens the residence time significantly. Values beyond h_{CCCT} do not have a significant impact on the residence time.

It was also shown that draw temperature has a significant impact on hardening time and can reduce residence time by 40% for each decrease of $4^{o}C$. Moreover, hardening a given volume with a central hole can lead to significant energy savings as it can reduce residence time by 50%. Furthermore, slicing a volume into thinner sections is an even more effective method to decrease hardening time.

2.2. PBM Hardening

Further study of the hardening process was performed through the application of population balance equations (PBE). Accurately modeling ice cream heat transfer and phase change is a challenging endeavor. The process has been simulated in Chapter 4 through a three-part model progression. Each step of the development has been validated through comparison with previously published experimental results. The crystalline microstructure has been predicted through a combination of commercial heat transfer and population balance software with user-defined functions for crystal nucleation and growth. The final simulated average crystal length of 35 μm is smaller than the 40-55 μm range reported in the literature (Russell et al., 1999), though the value is reasonably accurate. The work shows that PBE are becoming a viable design tool for the ice cream manufacturer. The method presented is flexible and efficient for determining the crystal size distribution (CSD) throughout the hardening process. The computational approach is applicable for numerous food-freezing processes, alloy solidification, and other multiphase systems.

2.3. CFD-PBE Freezing

Chapter 4 presented an efficient and flexible approach for combining computational fluid dynamics (CFD) with PBE. The add-on module available through Fluent captures the versatility of PBE in a straightforward manner. Model conditions can be varied quickly to yield satisfactory results. The model presented in Chapter 4 shows that PBE can be used to predict the CSD of a dynamic fluid in a scraped surface heat exchanger (SSHE). This information allows for crystal size and quality to be determined. The study serves as a baseline for varying phase properties, which will in turn provide a bridge for modeling the complex material properties of the ice cream mix.

3. Future Work

Any numerical simulation of a real-world process must be based upon certain idealizations or assumptions. The important aspect is the usefulness of the model being studied. The models presented in this thesis are useful for parametric study of energy efficiency in the hardening process and product quality (crystal size) in both the freezing and hardening processes. To obtain end-to-end energy efficiency analysis, it would be beneficial to model each process step in conjunction with one another. Moreover, greater information can be obtained by also including the storage process step. Additionally, further experimental study of ice cream crystallization kinetics is required to produce a more accurate CSD. Each of these advancements takes time to develop, and significant progress has been made through previous studies as well as in the current work.

References for Chapter 5

Russell AB, Cheney PE, Wantling SD. 1999. Influence of Freezing Conditions on Ice Crystallisation in Ice Cream. J Food Eng 39:179-91.

Tracey PH, McCown CY. 1934. A study of factors related to the hardening of ice cream. J Dairy Sci 17:47-60.

Appendix A - Thesis Publications

Cromer WC, Miller MJ, Xin XJ, Pei ZJ, Schmidt KA. Effects of Container Geometry on Energy Consumption During Hardening in Ice Cream Manufacturing. Proc MSEC 2010, Ed. ASME, Erie, Pennsylvania, USA, 2010 Oct 12-15th.

Miller MJ, Xin XJ, Pei ZJ, Schmidt KA. Ice Crystallization in Ice Cream Manufacturing by Coupled Computational Fluid Dynamics and Population Balance Method. Proc MSEC 2010, Ed. ASME, Erie, Pennsylvania, USA, 2010 Oct 12-15 th.

Miller MJ, Xin XJ, Pei ZJ, Schmidt KA. 2011. Investigation of Ice Cream Hardening Process by Finite Element Method. Int J of Refrig, Submitted.

Miller MJ, Xin XJ, Pei ZJ, Schmidt KA. 2011. Population Balance Model for Ice Cream Hardening. Comp Mat Sci, Submitted.

Rauth NL, Miller MJ, Xin XJ, Pei ZJ, Schmidt KA. Effects of Air Flow, Draw Temperature and Boundary Conditions on Hardening in Ice Cream Manufacturing. Proc MSEC 2010, Ed. ASME, Erie, Pennsylvania, USA, 2010 Oct 12-15th.

Appendix B - Calculation of Convective Heat Transfer Coefficient

The average convective heat transfer coefficient for a typical conveyor blast freezer is estimated here. Fluid properties and correlation equations were retrieved from published data (Incropera et al., 2007), and the freezer dimensions were taken from an actual field unit (Food Processing Equipment, 2009). The following assumptions were made:

1. Steady state flow conditions.
2. Constant properties.
3. Channel flow between and above ice cream packages; see diagram below.

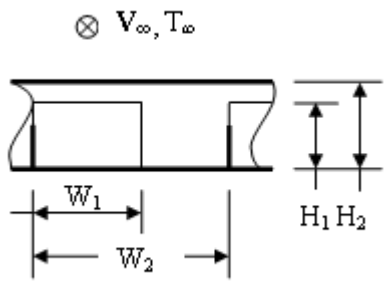

Figure B.1

The above figure is a schematic of the ice cream conveyer belt.

The average surface temperature is determined using the initial and final temperatures.

$$T_s = \frac{T_i + T_f}{2} \cong \frac{267 + 255}{2} K = 261\,\mathrm{K}$$

The total average or mean temperature is calculated using T_s and the fluid temperature.

$$T_m = \frac{T_\infty + T_s}{2} \cong \frac{239 + 261}{2} K = 250\,\mathrm{K}$$

The hydraulic diameter, D_H, is first calculated for subsequent equations.

$$D_H \equiv \frac{4 \cdot A_C}{P_W} \cong \frac{4[(0.1113)\cdot(0.4064)-(0.1)\cdot(0.12)]}{2(0.1113+0.4064)} = 0.1284\,(\mathrm{m})$$

The Reynolds number is next calculated to determine the flow type.

$$R_{e_D} \equiv \frac{V_\infty \cdot D_H}{\nu_f} \cong \frac{\left(5\,\mathrm{m/s}\right)\cdot(0.1284\mathrm{m})}{11.44\times10^{-6}\,\mathrm{m^2/s}} = 5.61\times10^4$$

Since R_{e_D} is larger than 10^4, the flow is turbulent.

Note that the flow is not fully developed, that is $\frac{L}{D_H} \cong 4.7$. Fully developed flow is typically observed at length-to-diameter ratios greater than 10, but the correlation shown below will still provide a reasonable value for the conditions used in this study. For short 'tubes' such as the one considered here, the average Nusselt number $\overline{Nu}_D$ will actually be larger than $Nu_{D,fd}$. Now an appropriate Nusselt Number correlation can be chosen, such as the Dittus-Boelter Equation.

$$Nu_D = 0.023\left(R_{e_D}\right)^{0.8}\cdot(\mathrm{Pr})^n$$

Where n = 0.3 for cooling $(T_s > T_\infty)$. Substituting in values yields: $Nu_D = 131.3$

Since $Nu_D \equiv \frac{h \cdot D_H}{k_f}$, rearranging for h and substituting in proper values gives: $h \cong 23$ W/(m^2·K). This value compares well with that given by Fellows (2000) of 25~30 W/(m^2·K).